Geosphere, published online on 12 January 2012 as doi:10.1130/GES00534.1

**Geosphere**

## Source-side shear-wave splitting and upper-mantle flow beneath the Arakan slab, India-Asia-Sundalind triple junction

R.M. Russo

*Geosphere* published online 12 January 2012;
doi: 10.1130/GES00534.1



**Notes**

Geosphere, published online on 12 January 2012 as doi:10.1130/GES00534.1

# Source-side shear-wave splitting and upper-mantle flow beneath the Arakan slab, India-Asia-Sundalind triple junction

**R.M. Russo***
*Department of Geological Sciences, P.O. Box 112120, Williamson 241, University of Florida, Gainesville, Florida 32611, USA*

## ABSTRACT

**Shear-wave splitting of *S* waves from earthquakes in the Arakan slab is consistent with strong asthenospheric anisotropy that developed as a consequence of the India-Asia collision. Global positioning system (GPS) site velocities in the India-Asia-Sundaland triple junction region show that deformation along the Arakan subduction zone is partitioned into dextral strike-slip motion, as India moves northwards with respect to Asia, and contraction across the Arakan trench and Chittagong-Tripura fold belt. Indian Ocean lithosphere comprising the Arakan slab is dismembered into three segments as a result of its collision with Asian lithosphere at the East Himalayan syntaxis. Offsets of intermediate-depth earthquake hypocenters at two locations delineate slab segments that form a left-stepping en echelon structure. Arakan slab focal mechanisms are consistent with slab sinking and along-strike compression and bending, and, south of 25°N, dextral strike-slip along the slab. Two regions of N-S contraction within the slab appear to be localized at the slab segment offsets. Teleseismically recorded *S* waves from earthquakes within the three slab segments, and surroundings, are split systematically: once corrected for receiver-side splitting, fast shear trends are predominantly trench-parallel beneath the east-dipping slab segments; are more nearly trench-normal on the Sundaland (east) side of the Arakan lithosphere; parallel the southern ~E-W gap between Arakan slab segments; and turn sharply around the extreme northern and southern edges of subducted Arakan lithosphere. Source-side shear-wave splitting beneath India is consistent with observed ~E-W–trending fast shear polarizations of *SK(K)S* splitting in northeastern India. The general pattern of both surface site velocities from GPS and shear-wave splitting studies is consistent with material flow around the eastern Himalayan syntaxis and into the mantle wedge above the Arakan slab, and around the northern terminus of the Arakan slab. The upper mantle may also flow through the gap between the central and southern Arakan slab segments.**

*E-mail: rrusso@ufl.edu

## ARAKAN SLAB AND INDIA-ASIA-SUNDALAND TRIPLE JUNCTION REGION

Despite its ongoing collision with Asia, begun in the Paleogene (e.g., Beck et al., 1995; Patzelt et al., 1996; Najman et al., 2008), India still moves northward some 3.9 cm/yr with respect to stable Eurasia (Socquet et al., 2006). Along its eastern boundary, the Indian plate subducts beneath western Sundaland (here, Indochina, Malaysia, and western Indonesia; Figs. 1 and 2) with varying, but high, obliquity along the Andaman (Vigny et al., 2005) and Arakan trenches (Cummins, 2007). Relative motion between India and overriding Indochina at the surface is dominantly dextral strike slip with some transpression along the Arakan portion of the subduction zone in Myanmar (Chamot-Rooke and Le Pichon, 1999; Simons et al., 1999, 2007; Michel et al., 2001; Nielsen et al., 2004; Socquet et al., 2006). Although the partitioning of GPS-determined deformation between permanent strain and elastic seismic cycle strain is unclear in Myanmar (but see Jade et al., 2007), geologic evidence for transpression and eastward subduction along the Arakan portion of the India-Sundaland includes well-exposed late Mesozoic ophiolite sequences (Acharyya, 2007), Neogene–Holocene deformation in the Chittagong-Tripura fold belt (Le Dain et al., 1984; Alam et al., 2003), active deformation of marine sediments in the Bay of Bengal segment of the subduction zone (Nielsen et al., 2004), and Quaternary–Holocene arc volcanoes developed on overriding Sunda lithosphere in central Myanmar (Maury et al., 2004). In addition, seismicity defines a well-developed east-dipping Wadati-Benioff zone down to ~150 km (Ni et al., 1989; Guzman-Speziale and Ni, 1996; Dasgupta et al., 2003; Rao and Kalpna, 2005; Stork et al., 2008; Figs. 2 and 3), and N-S–striking thrust focal mechanisms of shallow earthquakes occur in the Chittagong-Tripura fold belt and Central Burma Basin (Fig. 4). At least one large-magnitude subduction earthquake is known to have occurred on the southern Arakan plate interface, in 1762 (Cummins, 2007). Travel-time inversions of arrivals at global seismic networks and regional stations in India, Tibet, and Yunnan indicate that the Arakan slab penetrates to a depth of 300–400 km, and may then flatten beneath Indochina (Li et al., 2008).

### Arakan Slab Segmentation

Joint hypocentral relocations of Arakan slab earthquakes by Stork et al. (2008) show that the intermediate depth events are offset by nearly 100 km at two locations beneath Myanmar (Fig. 3). Whether these slab offsets represent contortions or tears in the slab at depths of 75–150 km is not clear, but that the Arakan slab is segmented, forming a set of three left-stepping en echelon portions, is unequivocal. Centroid moment-tensor focal mechanisms (Ekstrom et al., 2006) of Arakan slab events deeper than 40 km (Figs. 5 and 6) show that the slab is simultaneously sinking into the mantle (dip-slip events with ~N-S strike), bending due to along-strike compression (mixed thrust and strike-slip mechanisms with W-plunging neutral axes; Le Dain et al., 1984; Ni et al., 1989; see Russo et al., 1993, for an explanation of the basic mechanism of this type of slab lateral bending), and south of 25°N, a few mechanisms with dextral strike slip on generally N-striking nodal planes appropriate to shear due to India's northward motion. Note that a group of these earthquakes that occurred within the region of the northern Arakan slab offset (~25°N, 95.4°E) have nearly pure thrusting mechanisms with WNW-ESE–striking nodal planes (Fig. 6), and Ni et al. (1989) published very similar focal mechanisms for two events

*Geosphere*; February 2012; v. 8; no. 1; doi:10.1130/GES00534.1; 16 figures; 3 tables.

Geosphere, published online on 12 January 2012 as doi:10.1130/GES00534.1



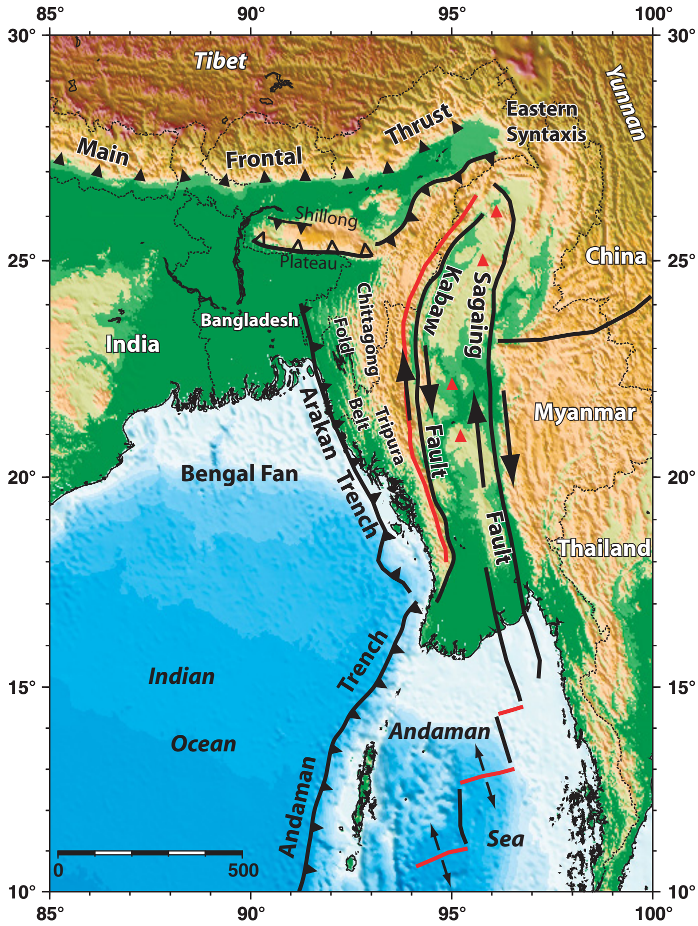


Figure 1. Map of the India-Asia-Sundaland triple junction region: heavy black lines are major faults; heavy red line marks the high topography of the Indo-Burman ranges. Andaman Sea spreading simplified from Curray (2005) and Khan and Chakraborty (2005). Red triangles are Cenozoic volcanic centers. Other geology from Bilham and England (2001), Clark and Bilham (2008), and works cited in main text.

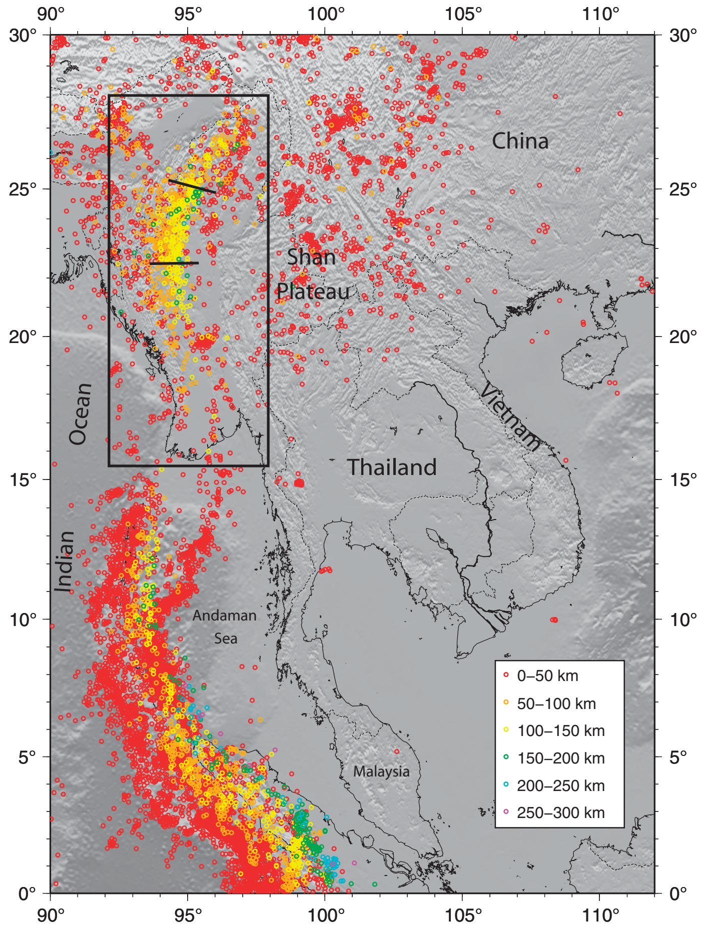


Figure 2. Seismicity of the study region, U.S. Geological Survey National Earthquake Information Center Catalog, 1963–2007. Event depths as per key, lower right. Approximate area of Figure 3 shown by box.

that occurred in the vicinity of the southern slab offset (~22°N, 95.5°E).

The Arakan slab segmentation (Stork et al., 2008), the observed along-strike lateral compression (Le Dain et al., 1984; Ni et al., 1989), and prevalence of slab-bending earthquakes deeper than 70 km would be expected, given India's relatively rapid northward motion (Le Dain et al., 1984), if such motions drive the northern terminus of the Arakan slab into the East Himalayan syntaxis. Figure 7 shows a conceptual model of the slab segmentation and development of the left-stepping en echelon offsets based on the precise relocations of Stork et al. (2007) and the internal slab deformation indicated by available focal mechanisms. Slab contortion or tearing at the two offset locations allows clockwise rotation of the slab segments about steep axes, thus increasing the bending of the slab and shortening its effective length. The combination of N-S compression along the slab at the segment offsets and the general dextral shear couple produced by India's northward motion result in the classic en echelon secondary shear-band deformation of a competent layer in a weaker medium (e.g., Ramsay and Lisle, 2000, see their figures 34.12, 34.15, and accompanying discussion), albeit at subducted slab scale.

The deformation of the Arakan slab, apparently a result of the ongoing India-Asia collision, is a clear indication that the interaction of the two plates affects not only a wide region at the surface, involving crustal motion around the East Himalayan syntaxis and southeastward extrusion of Indochina (e.g., Molnar and Tapponnier, 1975, 1977; Tapponnier et al., 1982; Le Dain et al., 1984; Shen et al., 2005; Zhang et al., 2005; Tanaka et al., 2008), but also extends to considerable depth. Gradients of mantle isotopic tracers ranging from high concentrations beneath China and Tibet and diminishing systematically around the syntaxis indicate that apparent crustal flow was matched by similar upper-mantle extrusion (Flower et al., 1998, 2001; Deng et al., 2004). The form of upper-mantle deformation at depths down to the top of the transition zone (410 km) can be discerned from seismic anisotropy detailed using shear-wave splitting analyses (e.g., Silver, 1996; Savage, 1999). Recent work on splitting of *SK(K)S* and similar core-traversing waves shows that the continent-continent collision entails surface and upper-mantle material flow around the East Himalayan syntaxis from southeastern Tibet and Yunnan to an approximately E-W zone at ~26°N beneath northern Indochina

Geosphere, published online on 12 January 2012 as doi:10.1130/GES00534.1



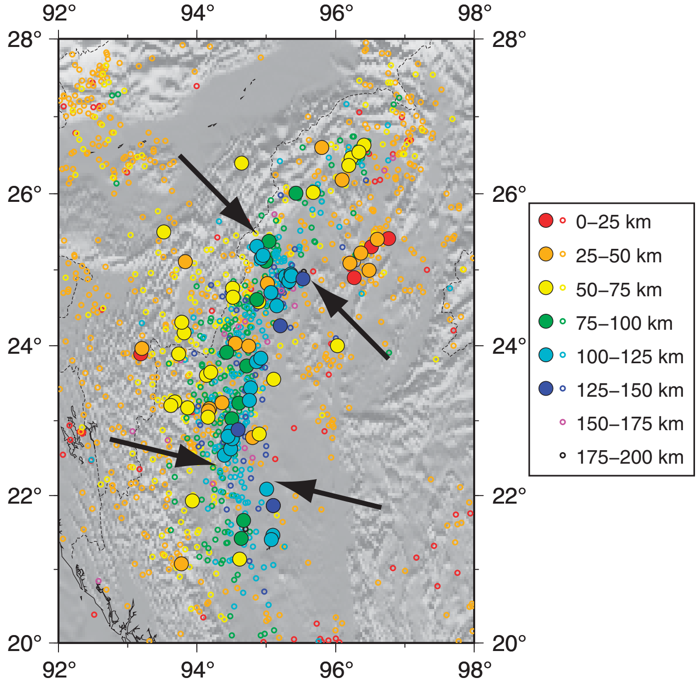


**Figure 3. Arakan slab seismicity and joint hypocenter determination relocations of Stork et al. (2008) (larger symbols). Event depth as per key, right. Background seismicity from the U.S. Geological Survey National Earthquake Information Center Catalog, 1963–2007. Arrows mark the two offsets in intermediate depth earthquakes, defining the three Arakan slab segments.**

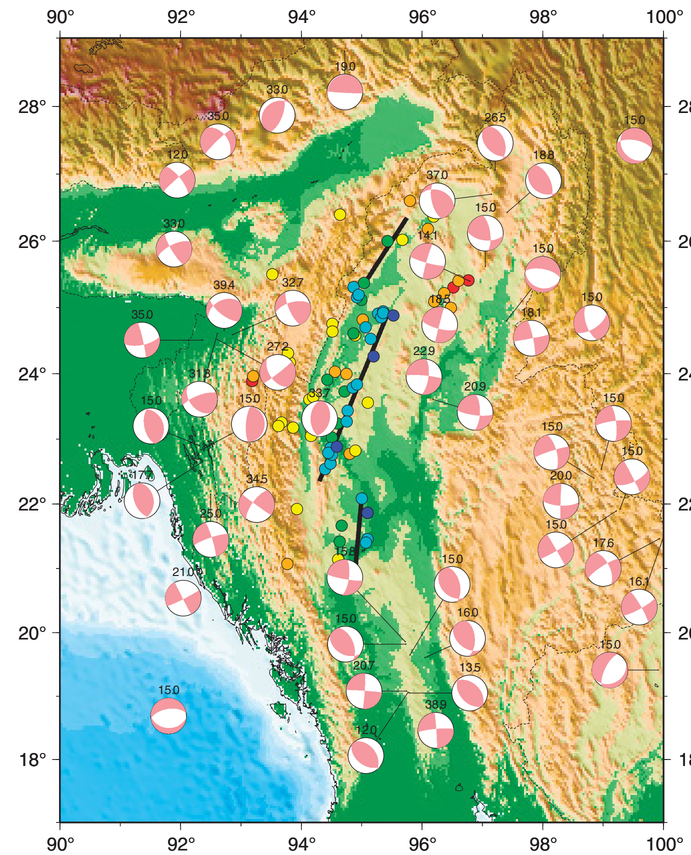


**Figure 4. Centroid moment tensor focal mechanisms (1990–2008) for shallow earthquakes (0–40 km) of the triple junction region. Source: U.S. Geological Survey National Earthquake Information Center. Individual event depths noted at the top of each mechanism.**

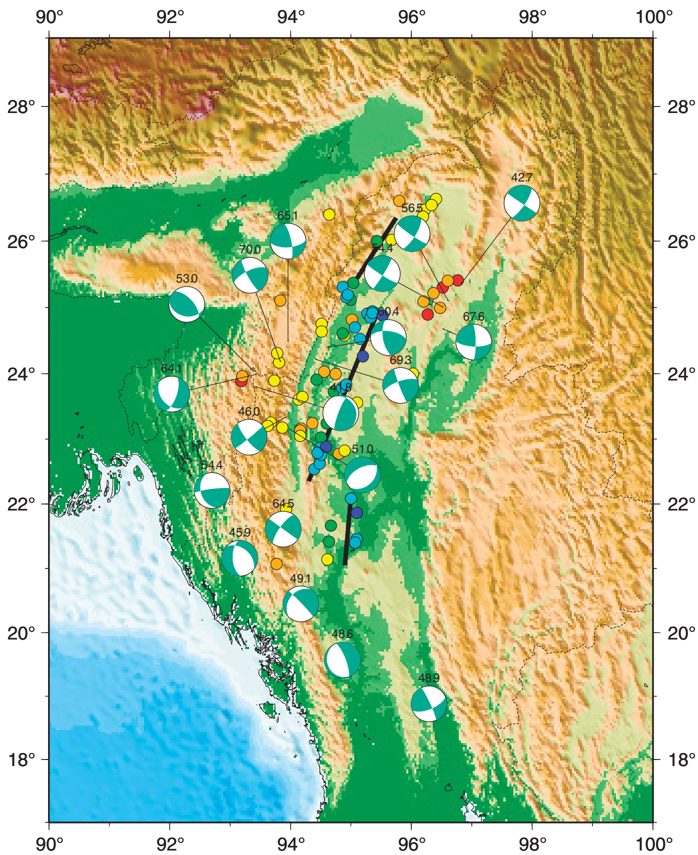


**Figure 5. Centroid moment tensor focal mechanisms (1990–2008) for events 40–70 km deep in the triple junction region. Source: U.S. Geological Survey National Earthquake Information Center. Individual event depths noted at the top of each mechanism.**

Geosphere, published online on 12 January 2012 as doi:10.1130/GES00534.1



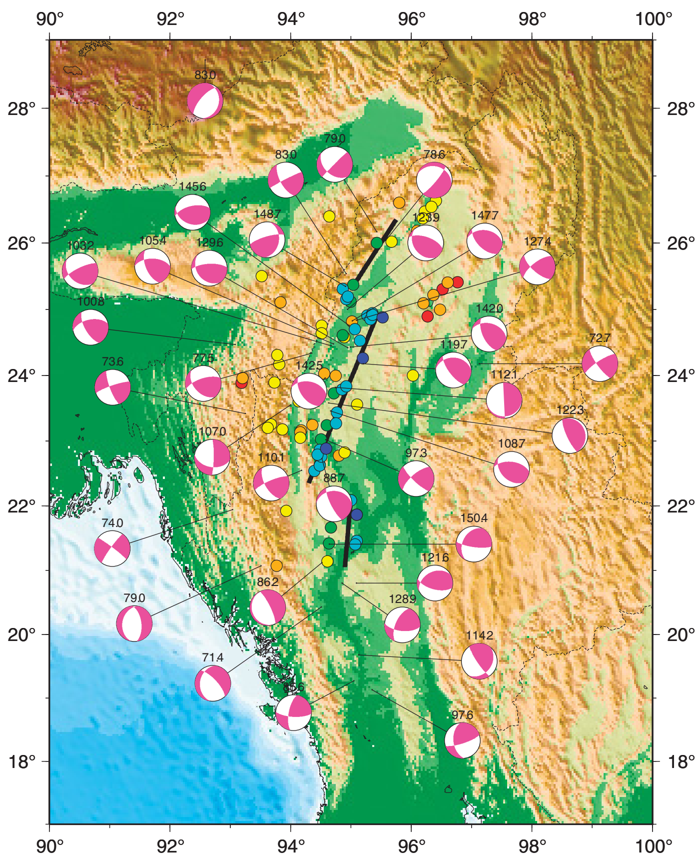


**Figure 6. Centroid moment tensor focal mechanisms (1990–2008) for events deeper than 70 km in the triple junction region. Source: U.S. Geological Survey National Earthquake Information Center. Individual event depths noted at the top of each mechanism.**

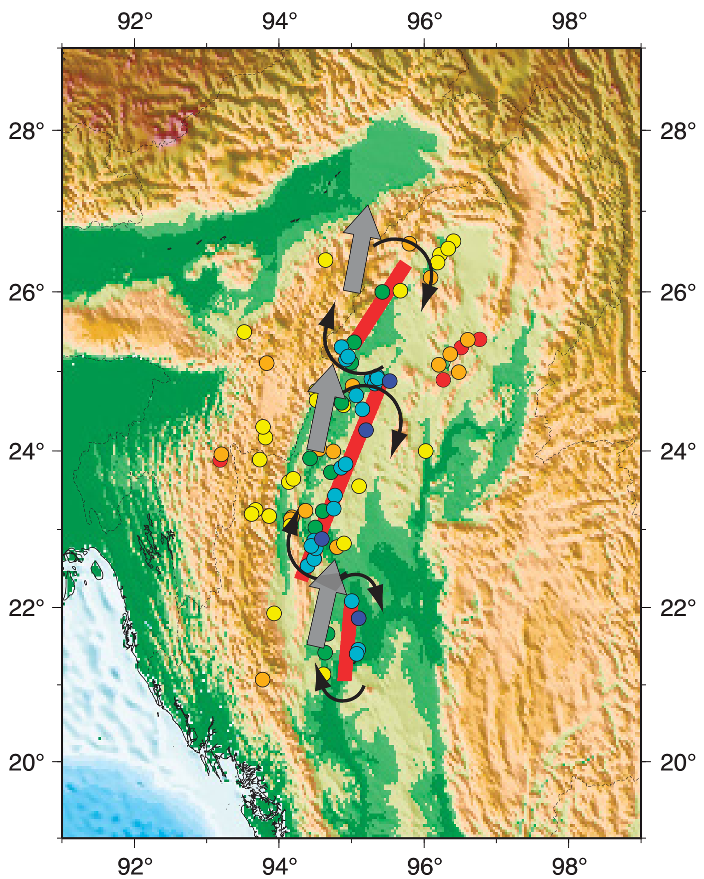


**Figure 7. Conceptual model for development of the three en echelon segments of the Arakan slab. Earthquake epicenters of Stork et al. (2008) also shown; depths as per key, Figure 3. Large gray arrows are India's motion with respect to Sundaland (Socquet et al., 2006). Heavy red lines mark the approximate extents along strike of the three segments. Thin black arrows show the clockwise sense of rotation about steep axes for each of the three segments.**

TABLE 1. EARTHQUAKE LOCATIONS

| Year | Julian day | Origin time | Latitude (°N) | Longitude (°E) | Depth (km) | Magnitude ($M_w$) |
|---|---|---|---|---|---|---|
| 1990 | 009 | 18:51:29.2 | 24.753 | 95.241 | 119.2 | 6.3 |
| 1992 | 106 | 01:32:09.9 | 24.315 | 94.898 | 116.1 | 5.7 |
| 1994 | 215 | 15:00:00.5 | 21.492 | 94.005 | 62.0 | 5.8 |
| 1994 | 220 | 21:08:31.6 | 24.721 | 95.200 | 121.7 | 6.1 |
| 1995 | 126 | 01:59:07.1 | 24.987 | 95.294 | 117.5 | 6.4 |
| 1996 | 316 | 09:22:27.7 | 19.330 | 95.013 | 80.0 | 6.0 |
| 1997 | 325 | 11:23:06.3 | 22.212 | 92.702 | 54.0 | 6.1 |
| 1997 | 364 | 13:43:18.6 | 25.384 | 96.609 | 33.0 | 5.8 |
| 1998 | 122 | 08:36:50.1 | 24.932 | 95.311 | 121.5 | 5.5 |
| 2000 | 285 | 09:42:09.2 | 23.866 | 94.863 | 116.5 | 5.6 |
| 2002 | 338 | 11:30:51.8 | 19.404 | 94.484 | 33.0 | 5.9 |
| 2004 | 344 | 08:49:00.5 | 24.711 | 92.523 | 38.5 | 5.5 |
| 2005 | 261 | 07:26:00.3 | 24.643 | 94.807 | 88.4 | 5.8 |
| 2006 | 131 | 17:22:54.0 | 23.297 | 94.261 | 44.1 | 5.4 |
| 2008 | 209 | 22:42:07.5 | 23.566 | 94.761 | 112.1 | 5.5 |

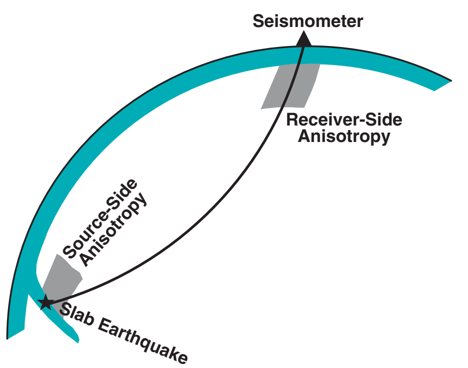


**Figure 8. Schematic *S* wave travel path showing two possible sources of splitting.**

Geosphere, published online on 12 January 2012 as doi:10.1130/GES00534.1



TABLE 2. RECEIVER-SIDE SPLITTING CORRECTIONS

| Station | Latitude (°) | Longitude (°) | Φ (°) | δt (s) | Reference or note |
|---|---|---|---|---|---|
| ALE | 82.503 | –62.350 | 61 | 0.91 | Helffrich et al., 1994 |
| ANTO | 32.869 | 32.794 | 25 | 1.30 | Vinnik et al., 1992 |
| AQU | 42.354 | 13.402 | –35 | 0.98 | Schmid et al., 2004 |
| ARU | 56.400 | 58.600 | 68 | 0.94 | Silver and Chan, 1991 |
| ATD | 11.530 | 42.847 | 48 | 1.59 | Barruol and Ben Ismail, 2001 |
| BFO | 48.332 | 8.331 | 40 | 1.00 | Vinnik et al., 1994 |
| BNI | 45.052 | 6.679 | –31 | 0.97 | Schmid et al., 2004 |
| BORG | 64.747 | –21.327 | 20 | 0.60 | Bjarnason et al., 2002 |
| BRVK | 53.058 | 70.283 | 66 | 1.21 | This study |
| CAN | –35.321 | 148.999 | –67 | 1.09 | Barruol and Hoffman, 1999 |
| CART | 37.587 | –1.001 | 70 | 1.72 | Schmid et al., 2004 |
| CHTO | 18.814 | 98.944 | –75 | 1.65 | Flesch et al., 2005 |
| CMLA | 37.764 | –25.524 | –61 | 0.60 | Behn et al., 2004 |
| COL | 64.900 | –147.790 | –82 | 1.55 | Silver and Chan, 1991 |
| CRZF | –46.430 | 51.8612 | –32 | 0.55 | Behn et al., 2004 |
| CTAO | –20.090 | 146.250 | 40 | 1.00 | Vinnik et al., 1992 |
| DSB | 53.245 | –6.276 | 58 | 0.95 | Restivo and Helffrich, 1999 |
| ECH | 48.216 | 7.158 | 85 | 0.88 | Barruol and Hoffman, 1999 |
| EIL | 29.670 | 34.951 | 3 | 1.33 | Schmid et al., 2004 |
| ERM | 42.015 | 143.157 | 26 | 1.25 | Savage et al., 1996 |
| ESK | 55.317 | –3.205 | 74 | 1.07 | Helffrich et al., 1994 |
| FODE | 35.380 | 24.958 | –60 | 0.45 | Schmid et al., 2004 |
| FURI | 8.903 | 38.688 | 36 | 1.38 | Ayele et al., 2004 |
| GRFO | 49.691 | 11.220 | 90 | 0.70 | Vinnik et al., 1992 |
| GVD | 34.839 | 24.087 | 88 | 0.91 | Schmid et al., 2004 |
| HIA | 49.267 | 119.742 | –20 | 0.70 | Sandvol et al., 1992 |
| IDI | 35.288 | 24.890 | 3 | 0.40 | Schmid et al., 2004 |
| INU | 35.350 | 137.029 | –85 | 1.13 | Barruol and Hoffman, 1999 |
| ISP | 37.823 | 30.522 | 11 | 1.46 | Schmid et al., 2004 |
| JER | 31.772 | 35.197 | 8 | 1.36 | Schmid et al., 2004 |
| KEV | 69.755 | 27.007 | 70 | 1.10 | Vinnik et al., 1992 |
| KIV | 43.956 | 42.688 | 88 | 1.20 | Helffrich et al., 1994 |
| KMBO | –1.126 | 37.252 | –18 | 1.12 | Barruol and Ben Ismail, 2001 |
| KMI | 25.123 | 102.740 | 70 | 0.73 | Lev et al., 2006 |
| KONO | 59.649 | 9.598 | 20 | 0.80 | Vinnik et al., 1992 |
| KRIS | 35.178 | 25.503 | Null | Station | Schmid et al., 2004 |
| KWP | 49.631 | 22.707 | –81 | 0.82 | Wiejacz, 2001 |
| LSA | 29.700 | 91.150 | 70 | 0.19 | Iidaka and Niu, 2001 |
| LSZ | –15.276 | 28.188 | 16 | 0.73 | Barruol and Ben Ismail, 2001 |
| MA2 | –16.449 | –152.268 | 72 | 1.27 | Ayele et al., 2004 |
| MAHO | 39.896 | 4.266 | –60 | 0.68 | Schmid et al., 2004 |
| MAJO | 36.543 | 138.207 | –50 | 0.90 | Vinnik et al., 1992 |
| MBAR | –0.602 | 30.738 | 4 | 1.48 | Walker et al., 2004a |
| MDJ | 44.616 | 129.592 | –85 | 0.50 | Iidaka and Niu, 2001 |
| MORC | 49.776 | 17.546 | –51 | 0.83 | Wylegalla et al., 1999 |
| MRNI | 33.012 | 35.392 | 7 | 1.53 | Schmid et al., 2004 |
| MSEY | –4.674 | 55.479 | 32 | 1.02 | Behn et al., 2004 |
| NAI | –1.274 | 36.804 | –19 | 1.00 | Barruol and Ben Ismail, 2001 |
| NWAO | –32.927 | 117.237 | 60 | 1.50 | Vinnik et al., 1992 |
| OBN | 55.113 | 36.569 | –19 | 0.68 | Helffrich et al., 1994 |
| PAF | –49.351 | 70.213 | –77 | 1.34 | Behn et al., 2004 |
| PMG | –9.409 | 147.154 | –63 | 0.80 | This study |
| RAYN | 23.523 | 45.503 | 5 | 1.31 | Ayele et al., 2004 |
| RER | –21.159 | 55.746 | –81 | 0.77 | Behn et al., 2004 |
| RGN | 54.548 | 13.321 | 43 | 0.70 | Barruol and Ben Ismail, 2001 |
| RUE | 52.477 | 13.779 | –83 | 0.68 | Wylegalla et al., 1999 |
| SANT | 36.371 | 25.459 | 9 | 0.76 | Schmid et al., 2004 |
| SSB | 45.279 | 4.542 | –41 | 1.30 | Babuska et al., 2002 |
| STU | 48.772 | 9.195 | 50 | 0.50 | Vinnik et al., 1992 |
| SUW | 54.013 | 23.181 | –82 | 0.71 | Wiejacz, 2001 |
| TAM | 22.791 | 5.527 | –6 | 0.87 | Barruol and Ben Ismail, 2001 |
| TAU | –42.909 | 147.320 | 80 | 0.60 | Vinnik et al., 1992 |
| TIXI | 71.649 | 128.866 | –41 | 2.99 | Oreshin et al., 2002 |
| TLY | 51.681 | 103.644 | 70 | 1.00 | Barruol and Russo, 1996 |
| TRI | 45.709 | 13.764 | 56 | 0.73 | Schmid et al., 2004 |
| ULN | 47.865 | 107.053 | 52 | 0.60 | Liu et al., 2008 |
| VSL | 39.496 | 9.378 | 69 | 1.64 | Schmid et al., 2004 |
| VTS | 42.592 | 23.208 | –26 | 0.96 | Schmid et al., 2004 |
| WAKE | 19.283 | 166.654 | –49 | 1.20 | Garcia and Russo, 2005 |
| WDD | 35.867 | 14.523 | –65 | 0.83 | Schmid et al., 2004 |
| YAK | 62.031 | 129.681 | –34 | 1.24 | Oreshin et al., 2002 |
| YSS | 46.958 | 142.761 | 11 | 1.13 | Fouch and Fischer, 1996 |

Geosphere, published online on 12 January 2012 as doi:10.1130/GES00534.1



(Lev et al., 2006; Sol et al., 2007; Wang et al., 2008). Shear-wave splitting analyses from northeastern India are consistent with generally E-W upper-mantle fabrics south of Tibet and west of the syntaxis (Singh et al., 2006, 2007). These results were derived from data collected at temporary seismic deployments in China and India, and such deployments are not currently possible in Myanmar. However, the form of the upper-mantle deformation field south of the syntaxis in Myanmar and northeastern India can be determined using shear waves from earthquakes in the Arakan slab itself (e.g., Russo and Silver, 1994; Russo, 2009; Russo and Mocanu, 2009; Russo et al., 2010). In the following, I present results from such a study and show that the deformation of the Arakan slab strongly affects upper-mantle anisotropy locally, and that the larger-scale upper-mantle flow in the region is consistent with India's northward motion and flow around the northern and southern ends of the Arakan slab, and perhaps also through the southern slab gap.

## SOURCE-SIDE SHEAR-WAVE SPLITTING

Source-side shear-wave splitting measurements are made using teleseismic *S* waves (30° < Δ < 84°) recorded at global seismic network stations (i.e., Incorporated Research Institutions of Seismology [IRIS] Global Seismic Network [GSN], GEOSCOPE network, GEOFON network) whose substation upper-mantle shear-wave splitting parameters are known. These events must be large enough to be well recorded teleseismically ($M_w$ >5.5) and deeper than 40 km to ensure that the reflected phases *pS* and *sS* do not arrive simultaneously with the long-period (10 s) direct *S* wave. Since 1990, when the broadband global network began to come online, 15 suitable Arakan slab events have occurred (Table 1). One of these events, the earthquake on Julian day 364 during 1997, occurred at a depth shallower than 40 km, but examination of *S* waves from the event shows little or no evidence of contamination by *pS* or *sS*, so it was also used in the study.

Shear-wave splitting that occurs along the downgoing travel path from the Arakan slab can be isolated because these *S* waves turn in the largely isotropic lower mantle (Meade et al., 1995). Shear-wave splitting at the core-mantle boundary (CMB) region appears to be small (e.g., Hall et al., 2004), and could potentially affect only the few *S* waves used in the study that travel to the extreme of the distance range (80°–84°). Contributions to splitting from the upper mantle deeper than the olivine stability field is infrequently observed and is attributed to

TABLE 3. SOURCE-SIDE SPLITTING MEASUREMENTS

| Station | Distance (°) | Azimuth (°) | Φ (°) | δt (s) | Result |
|---|---|---|---|---|---|
| **09 January 1990 (90009)** | | | | | |
| ARU | 41.3 | 329.8 | 175 ± 10 | — | Null |
| HIA | 31.1 | 31.8 | –28 ± 14 | 3.05 ± 0.55 | Measurement |
| INU | 37.4 | 63.6 | –39 ± 7 | 2.10 ± 0.18 | Measurement |
| KMI | 6.8 | 85.3 | 16 ± 4 | 2.20 ± 0.13 | Measurement |
| OBN | 52.2 | 321.6 | 42 ± 16 | 0.95 ± 0.18 | Measurement |
| SSB | 73.3 | 312.5 | –78 ± 21 | 3.60 ± 0.63 | Measurement |
| **15 April 1992 (92106)** | | | | | |
| ALE | 72.8 | 357.9 | 155 ± 23 | — | Null |
| ERM | 43.5 | 53.9 | 162 ± 23 | — | Null, corrected |
| KIV | 46.6 | 308.2 | 42 ± 10 | 2.65 ± 0.48 | Measurement |
| LSA | 6.3 | 328.9 | 34 ± 23 | — | Null |
| MAJO | 39.0 | 61.4 | –23 ± 14 | 3.10 ± 0.35 | Measurement |
| NWAO | 60.8 | 158.5 | 55 ± 23 | — | Null |
| **03 August 1994 (94215)** | | | | | |
| ALE | 75.6 | 356.9 | 106 ± 23 | — | Null |
| ANTO | 54.7 | 304.3 | 25 ± 23 | — | Null |
| ATD | 49.8 | 267.1 | 71 ± 23 | — | Null |
| CHTO | 5.4 | 119.0 | 20 ± 23 | — | Null |
| CTAO | 65.7 | 125.4 | –38 ± 4 | 3.75 ± 0.83 | Measurement |
| DSB | 79.0 | 323.0 | –10 ± 11 | 5.10 ± 1.05 | Measurement |
| ESK | 76.6 | 324.3 | 5 ± 15 | 4.05 ± 0.78 | Measurement |
| GRFO | 69.3 | 316.5 | 17 ± 9 | 4.20 ± 0.40 | Measurement |
| HIA | 34.4 | 30.2 | 13 ± 23 | — | Null |
| KEV | 62.1 | 338.7 | 19 ± 20 | 0.80 ± 0.68 | Measurement |
| KIV | 47.8 | 310.4 | –21 ± 8 | 4.20 ± 1.10 | Measurement |
| KONO | 68.9 | 327.2 | –5 ± 13 | 3.35 ± 0.48 | Measurement |
| MAJO | 41.1 | 58.7 | –80 ± 8 | 4.75 ± 0.30 | Measurement |
| NWAO | 58.5 | 157.1 | –64 ± 10 | 2.85 ± 0.50 | Measurement |
| OBN | 54.1 | 323.3 | –8 ± 18 | 5.20 ± 0.70 | Measurement |
| PET | 57.9 | 40.1 | 75 ± 23 | — | Null |
| PMG | 60.5 | 114.9 | –24 ± 17 | 2.65 ± 0.53 | Measurement |
| STU | 70.8 | 315.8 | 6 ± 23 | — | Null |
| WRAB | 57.0 | 133.4 | 45 ± 23 | — | Null |
| YAK | 47.3 | 22.0 | 22 ± 23 | — | Null |
| YSS | 46.7 | 45.1 | 61 ± 13 | 4.60 ± 0.60 | Measurement |
| **08 August 1994 (94220)** | | | | | |
| ALE | 72.4 | 357.0 | 63 ± 2 | — | Null |
| ANTO | 53.9 | 302.4 | –1 ± 18 | 0.85 ± 0.93 | Measurement |
| ARU | 41.3 | 329.9 | 63 ± 23 | — | Null |
| ATD | 51.2 | 265.0 | 17 ± 23 | — | Null |
| BORG | 78.4 | 336.9 | 58 ± 23 | — | Null |
| COL | 78.5 | 22.8 | 16 ± 23 | — | Null |
| CTAO | 66.7 | 127.3 | 87 ± 11 | 1.85 ± 0.73 | Measurement |
| ESK | 74.6 | 324.1 | 24 ± 9 | 1.55 ± 0.20 | Measurement |
| GRFO | 67.8 | 315.8 | 64 ± 23 | — | Null |
| HIA | 31.1 | 31.8 | –19 ± 8 | 4.85 ± 1.00 | Measurement |
| KEV | 59.5 | 338.0 | –40 ± 7 | 2.05 ± 0.73 | Measurement |
| KIV | 46.6 | 307.9 | 17 ± 5 | 2.95 ± 0.18 | Measurement |
| KONO | 66.8 | 326.6 | –18 ± 18 | 2.15 ± 0.53 | Measurement |
| LSZ | 76.5 | 246.0 | 24 ± 23 | — | Null |
| MDJ | 34.2 | 45.9 | 87 ± 23 | — | Null |
| STU | 69.3 | 315.1 | 66 ± 23 | — | Null |
| MAJO | 38.5 | 61.8 | –47 ± 11 | 2.65 ± 0.25 | Measurement |
| OBN | 52.2 | 321.6 | –21 ± 7 | 3.60 ± 0.65 | Measurement |
| **06 May 1995 (95126)** | | | | | |
| ALE | 72.2 | 357.0 | 58 ± 2 | 4.70 ± 0.28 | Measurement |
| ARU | 41.1 | 329.7 | 58 ± 23 | — | Null |
| ATD | 51.3 | 264.8 | 63 ± 23 | — | Null |
| BORG | 78.2 | 336.9 | 46 ± 9 | 3.65 ± 0.11 | Measurement |
| CAN | 78.6 | 137.8 | 61 ± 7 | 2.15 ± 0.23 | Measurement |
| CHTO | 7.0 | 150.4 | –89 ± 4 | 3.20 ± 0.30 | Measurement |
| COL | 78.2 | 22.9 | 79 ± 4 | — | Null, corrected |
| CTAO | 66.8 | 127.4 | 18 ± 23 | — | Null |
| ECH | 70.6 | 314.9 | 25 ± 23 | — | Null, corrected |
| GRFO | 67.6 | 315.7 | 36 ± 23 | — | Null |
| INU | 37.3 | 63.9 | –32 ± 11 | 2.95 ± 0.40 | Measurement |
| KIV | 46.5 | 307.7 | –57 ± 7 | 3.40 ± 0.58 | Measurement |

(*continued*)

TABLE 3. SOURCE-SIDE SPLITTING MEASUREMENTS (*continued*)

| Station | Distance (°) | Azimuth (°) | Φ (°) | δt (s) | Result |
|---|---|---|---|---|---|
| | | **06 May 1995 (95126)** (*continued*) | | | |
| KONO | 66.6 | 326.5 | 28 ± 8 | 2.75 ± 0.78 | Measurement |
| MA2 | 51.4 | 32.4 | –63 ± 14 | 2.90 ± 0.40 | Measurement |
| MBC | 76.7 | 8.0 | 1 ± 4 | — | Null |
| MDJ | 34.0 | 46.1 | 11 ± 23 | — | Null |
| NAI | 62.3 | 254.3 | 52 ± 5 | — | Null |
| OBN | 52.1 | 321.5 | 88 ± 23 | — | Null |
| STU | 69.2 | 315.1 | 23 ± 23 | — | Null |
| YSS | 43.4 | 47.2 | –13 ± 12 | 3.75 ± 0.93 | Measurement |
| | | **11 November 1996 (96316)** | | | |
| ARU | 46.9 | 332.7 | 84 ± 23 | — | Null |
| BFO | 73.6 | 316.0 | 75 ± 23 | — | Null |
| CHTO | 3.8 | 97.2 | –65 ± 8 | 3.65 ± 0.98 | Measurement |
| CRZF | 76.2 | 209.2 | –71 ± 16 | 1.40 ± 0.58 | Measurement |
| CTAO | 63.7 | 125.1 | –66 ± 3 | 4.55 ± 0.45 | Measurement |
| ECH | 74.4 | 316.1 | 79 ± 23 | — | Null |
| ERM | 46.5 | 50.0 | 52 ± 23 | — | Null |
| ESK | 78.9 | 324.8 | 27 ± 23 | — | Null |
| INU | 40.3 | 57.8 | –9 ± 11 | 3.30 ± 0.60 | Measurement |
| ISP | 58.5 | 303.0 | 81 ± 23 | — | Null |
| JER | 54.8 | 295.7 | 80 ± 9 | 2.25 ± 0.48 | Measurement |
| KEV | 64.4 | 339.0 | 41 ± 23 | — | Null |
| KIV | 49.9 | 311.6 | 12 ± 23 | — | Null |
| KONO | 71.2 | 327.7 | 69 ± 10 | — | Null |
| MDJ | 38.2 | 40.9 | 53 ± 23 | — | Null |
| NWAO | 56.1 | 157.5 | 7 ± 23 | — | Null |
| OBN | 56.4 | 324.0 | 88 ± 10 | — | Null |
| PAF | 71.8 | 196.8 | 77 ± 10 | — | Null |
| RAYN | 46.1 | 284.4 | 32 ± 10 | — | Null |
| RGN | 69.7 | 322.1 | 0 ± 13 | 2.80 ± 0.75 | Measurement |
| SSB | 76.8 | 313.5 | –29 ± 8 | 4.25 ± 0.92 | Measurement |
| STU | 73.0 | 316.4 | –27 ± 12 | 2.30 ± 0.73 | Measurement |
| SUW | 63.9 | 321.4 | 72 ± 23 | — | Null |
| TAU | 78.4 | 143.6 | 75 ± 17 | 1.15 ± 0.48 | Measurement |
| TLY | 33.0 | 9.9 | 30 ± 23 | — | Null |
| ULN | 30.1 | 16.3 | 22 ± 23 | — | Null |
| | | **21 November 1997 (97325)** | | | |
| ALE | 74.8 | 356.7 | 15 ± 23 | — | Null |
| ANTO | 53.3 | 303.8 | 23 ± 23 | — | Null |
| ATD | 48.7 | 265.9 | 76 ± 23 | — | Null |
| BFO | 70.1 | 315.1 | 28 ± 10 | — | Null |
| BORG | 79.8 | 336.5 | 24 ± 23 | — | Null |
| CAN | 78.2 | 136.0 | 52 ± 15 | 1.95 ± 0.58 | Measurement |
| CRZF | 77.7 | 207.6 | –5 ± 12 | 2.00 ± 0.48 | Measurement |
| CTAO | 67.1 | 124.8 | 6 ± 5 | 3.55 ± 0.65 | Measurement |
| ECH | 70.9 | 315.1 | 21 ± 23 | — | Null |
| EIL | 52.0 | 291.0 | 75 ± 23 | — | Null |
| ESK | 75.3 | 324.0 | 30 ± 23 | — | Null |
| FURI | 53.4 | 264.6 | 68 ± 23 | — | Null |
| GRFO | 68.0 | 316.1 | 6 ± 19 | 1.20 ± 0.65 | Measurement |
| INU | 40.7 | 61.2 | –29 ± 7 | 4.10 ± 0.42 | Measurement |
| JER | 51.6 | 293.6 | 22 ± 23 | — | Null |
| KMBO | 58.8 | 254.3 | –12 ± 8 | 2.55 ± 0.50 | Measurement |
| KONO | 67.6 | 327.0 | 31 ± 23 | — | Null |
| MA2 | 55.0 | 31.8 | –65 ± 13 | 4.10 ± 0.45 | Measurement |
| MDJ | 37.6 | 44.7 | –12 ± 7 | 3.45 ± 0.88 | Measurement |
| OBN | 52.8 | 323.2 | 39 ± 23 | — | Null |
| PAF | 74.0 | 21.6 | 15 ± 15 | 2.25 ± 0.90 | Measurement |
| RAYN | 43.4 | 281.2 | 22 ± 23 | — | Null |
| RGN | 66.1 | 321.2 | 90 ± 5 | 1.85 ± 0.08 | Measurement |
| STU | 69.4 | 315.4 | 23 ± 5 | — | Null |
| SUW | 60.3 | 320.5 | –64 ± 11 | 3.15 ± 0.80 | Measurement |
| TAM | 79.2 | 290.2 | 17 ± 23 | — | Null |
| WAKE | 68.6 | 77.2 | 88 ± 23 | — | Null |
| | | **30 December 1997 (97364)** | | | |
| ANTO | 54.6 | 302.1 | 65 ± 3 | — | Null, corrected |
| ARU | 41.4 | 328.8 | 9 ± 4 | 4.40 ± 0.28 | Measurement |
| ATD | 52.5 | 265.1 | –18 ± 4 | 3.10 ± 0.65 | Measurement |
| BFO | 70.4 | 314.9 | 66 ± 23 | — | Null, corrected |

(*continued*)

preferred alignment of wadsleyite (Fischer and Wiens, 1996; Fouch and Fischer, 1996; Wookey and Kendall, 2004). Shear-wave splitting due to upper-mantle substation anisotropy can be determined using *SK(K)S* and *PKS* phases, and thus the splitting on the receiver side of the *S*-wave travel path (Fig. 8) can be corrected (Russo and Silver, 1994; Russo, 2009; Russo and Mocanu, 2009).

Observed receiver station splitting parameters used to correct for splitting beneath the receiver stations are detailed in Table 2. Station splitting corrections were applied when clear splitting of Arakan event *S* waves was observed at the receiver stations; however, when no splitting was observed (i.e., a linear *S* wave, or null splitting), receiver corrections were not applied. Note, only one receiver station used in this study is considered to be isotropic (KRIS, Schmid et al., 2004), and thus never required correction for receiver-side splitting. Details of the method for correcting known station splitting can be found in Russo and Silver (1994), Russo (2009), and Russo and Mocanu (2009).

## RESULTS

The 15 suitable Arakan slab earthquakes (Table 1) yielded 103 receiver-corrected source-side splitting measurements and 152 null splitting observations (Table 3). Splitting nulls derive from observed linear waveforms—either before or after receiver splitting correction—and occur when either the initial *S*-wave polarization fortuitously parallels one of two possible anisotropic symmetry directions or the medium traversed is isotropic. An example of the splitting measurement before and after receiver correction is shown in Figure 9. Positive splitting results and nulls for each event are shown in Figure 10, and all splitting parameters are detailed in Table 3. The Arakan slab event that occurred on Julian day 209, 2008 (Table 1), yielded no suitable waveforms for splitting and will not be discussed further. Splitting delay times are generally high, with a mean of 3.0 s, similar to that found for source-side splitting in the Cascades region (2.9 s; Russo, 2009) and the Carpathian Arc (2.77 s; Russo and Mocanu, 2009). Results in Figure 10 are plotted at surface projections of the point at 200 km depth along their downgoing path from the source event to the receiver station. This procedure allows discernment of variable upper-mantle anisotropy in the source region (Russo, 2009; Russo and Mocanu, 2009), and is predicated on results of numerical studies of *S*-wave–effective Fresnel zones (Zhao et al., 2000) and the effects of slowly varying anisotropy on observed splitting (Saltzer et al., 2000).

Geosphere, published online on 12 January 2012 as doi:10.1130/GES00534.1



As is clear from Figure 10, shear-wave splitting in the vicinity of the Arakan slab is highly variable, and appears to depend strongly on the upper-mantle volume sampled by the downgoing *S* waves. The source earthquakes differ in both location and depth, although the majority of the earthquakes occurred in the central segment of the Arakan slab at depths of ~110–120 km. Typically, one of the two possible fast shear trends of observed splitting nulls, whether null before or after receiver splitting correction, is consistent with observed splitting fast axes for similar source-receiver paths. In several instances, I measured splitting of *S* waves recorded at stations at short distances from the source events (6°–8°). Although these waves could have acquired their splitting anywhere along their paths and are potentially subject to phase modifications due to shallow incidence (e.g., Crampin and Booth, 1985), results, once receiver corrected, are consistent with splitting measurements made at teleseismic station distances along similar azimuths (Figs. 10A, 10D, and 10E).

## DISCUSSION

### Shear-Wave Splitting and Upper-Mantle Anisotropy

Teleseismic shear-wave splitting is commonly associated with development of linear preferred orientation (LPO) in olivine-dominated upper-mantle aggregates. The LPO aligns olivine crystallographic *a*-axes (seismically fast) in the finite deformation shear plane parallel to the direction of tectonic extension (Hess, 1964; Carter et al., 1972; Gueguen and Nicolas, 1980; Christensen, 1984; Nicolas and Christensen, 1987; Ribe, 1989a, 1989b; Ribe and Yu, 1991; Zhang et al., 2000; Kaminski and Ribe, 2001; Jung et al. 2006). LPO in natural upper-mantle samples typically follows this basic type-A fabric (Mainprice and Silver, 1993; Ben Ismail and Mainprice, 1998), although petrographically distinct type-C and type-E fabrics that yield shear-wave splitting with fast polarizations in the material flow direction, similar to the A-type fabric, also exist (Jung et al., 2006).

The presence of water under high stress conditions may also complicate anisotropic fabrics, producing a distinctive B-type fabric (Jung and Karato, 2001; Karato, 2003; Jung et al., 2006), and the presence of melt apparently results in similar fabrics (Holtzman et al., 2003). Elevated water content and partial melt thus may modify LPO fabrics, yielding olivine *b*-axis concentrations in the shear plane and/or material extension direction, or girdles of crystallographic axes, instead of the usual *a*-axis clustering. Non-

TABLE 3. SOURCE-SIDE SPLITTING MEASUREMENTS (*continued*)

| Station | Distance (°) | Azimuth (°) | Φ (°) | δt (s) | Result |
|---|---|---|---|---|---|
| | | **30 December 1997 (97364)** (*continued*) | | | |
| CAN | 78.1 | 138.5 | –85 ± 18 | 2.45 ± 0.55 | Measurement |
| ECH | 71.2 | 315.0 | 74 ± 4 | — | Null, corrected |
| EIL | 54.3 | 289.4 | 35 ± 23 | — | Null, corrected |
| ESK | 74.8 | 324.3 | 36 ± 23 | — | Null, corrected |
| FURI | 57.3 | 264.2 | 71 ± 18 | — | Null, corrected |
| GRFO | 68.2 | 315.8 | 80 ± 20 | 1.15 ± 1.08 | Measurement |
| INU | 36.0 | 64.2 | –51 ± 6 | 4.50 ± 0.33 | Measurement |
| ISP | 56.6 | 299.9 | 26 ± 23 | — | Null, corrected |
| JER | 53.7 | 291.9 | 33 ± 23 | — | Null, corrected |
| KEV | 59.4 | 337.7 | –3 ± 13 | 3.60 ± 0.90 | Measurement |
| KMBO | 62.1 | 254.7 | 83 ± 4 | — | Null, corrected |
| KONO | 67.0 | 326.6 | 38 ± 23 | — | Null, corrected |
| KIV | 47.2 | 307.3 | 24 ± 4 | — | Null, corrected |
| MA2 | 50.5 | 32.3 | 61 ± 12 | 2.50 ± 0.38 | Measurement |
| MDJ | 32.7 | 45.8 | –47 ± 8 | 4.75 ± 0.83 | Measurement |
| NWAO | 61.2 | 160.2 | 3 ± 5 | — | Null, corrected |
| OBN | 52.5 | 321.2 | 29 ± 22 | — | Null, corrected |
| PAF | 78.0 | 197.3 | 25 ± 23 | — | Null, corrected |
| RAYN | 46.3 | 279.0 | –22 ± 17 | 3.20 ± 0.11 | Measurement |
| RGN | 65.9 | 320.7 | 37 ± 23 | — | Null |
| SSB | 73.8 | 312.7 | 36 ± 23 | — | Null |
| STU | 69.7 | 315.2 | 31 ± 23 | — | Null |
| YSS | 42.3 | 47.2 | –17 ± 7 | 1.95 ± 0.30 | Measurement |
| | | **02 May 1998 (98122)** | | | |
| ALE | 72.2 | 357.0 | 56 ± 4 | — | Null |
| ANTO | 53.8 | 302.2 | 80 ± 23 | — | Null |
| AQU | 67.9 | 307.6 | 81 ± 23 | — | Null |
| BFO | 69.9 | 314.8 | –8 ± 4 | 3.85 ± 0.48 | Measurement |
| BRVK | 33.9 | 332.7 | 11 ± 15 | 2.15 ± 0.50 | Measurement |
| CTAO | 66.8 | 127.4 | 58 ± 23 | — | Null |
| ERM | 42.8 | 54.4 | 74 ± 23 | — | Null |
| GRFO | 67.7 | 315.7 | 85 ± 4 | — | Null |
| GUMO | 47.9 | 94.1 | 11 ± 23 | — | Null |
| HIA | 30.9 | 31.9 | 46 ± 23 | — | Null |
| ISP | 55.8 | 300.0 | 78 ± 23 | — | Null |
| JER | 52.8 | 292.0 | 80 ± 23 | — | Null |
| KEV | 59.3 | 337.9 | 69 ± 1 | — | Null |
| KIV | 46.5 | 307.7 | 68 ± 14 | 3.20 ± 0.38 | Measurement |
| KONO | 66.7 | 326.5 | 81 ± 3 | 4.20 ± 0.75 | Measurement |
| MA2 | 51.5 | 32.4 | –57 ± 3 | 4.00 ± 0.35 | Measurement |
| MORC | 53.6 | 315.0 | 69 ± 23 | — | Null |
| OBN | 52.1 | 321.5 | 90 ± 23 | — | Null |
| | | **11 October 2000 (00285)** | | | |
| ALE | 73.3 | 357.0 | 29 ± 23 | — | Null |
| AQU | 68.2 | 307.9 | –17 ± 3 | 3.95 ± 0.22 | Measurement |
| ARU | 41.9 | 330.5 | 8 ± 23 | — | Null |
| FODE | 60.7 | 298.4 | 22 ± 19 | 1.90 ± 0.58 | Measurement |
| FURI | 55.6 | 264.4 | –5 ± 20 | 3.85 ± 0.80 | Measurement |
| HIA | 32.0 | 31.3 | 56 ± 23 | — | Null |
| INU | 38.1 | 62.7 | 89 ± 23 | — | Null |
| ISP | 56.0 | 300.6 | 4 ± 23 | — | Null, corrected |
| KEV | 60.2 | 338.2 | 22 ± 14 | — | Null, corrected |
| KIV | 46.9 | 308.6 | 87 ± 18 | 3.05 ± 0.48 | Measurement |
| MBAR | 66.7 | 258.4 | 15 ± 16 | 1.70 ± 0.50 | Measurement |
| MDJ | 35.0 | 45.2 | –24 ± 9 | 2.75 ± 0.50 | Measurement |
| MRNI | 52.5 | 294.3 | 77 ± 9 | 2.80 ± 0.68 | Measurement |
| RAYN | 45.0 | 280.0 | 10 ± 17 | 2.40 ± 0.50 | Measurement |
| RER | 58.8 | 223.5 | 41 ± 23 | — | Null |
| TIXI | 51.5 | 13.1 | 37 ± 7 | — | Null |
| YSS | 44.5 | 46.5 | 76 ± 23 | — | Null |
| | | **04 December 2002 (02338)** | | | |
| ANTO | 56.3 | 305.4 | 39 ± 10 | — | Null, corrected |
| BFO | 79.6 | 315.9 | 48 ± 23 | — | Null, corrected |
| CTAO | 64.1 | 124.9 | 40 ± 23 | — | Null |
| EIL | 54.6 | 293.0 | –53 ± 5 | 2.40 ± 0.40 | Measurement |
| GUMO | 48.5 | 88.8 | 67 ± 23 | — | Null |
| HIA | 36.0 | 28.4 | –57 ± 21 | 1.10 ± 0.80 | Measurement |
| JER | 54.3 | 295.6 | 26 ± 4 | 1.55 ± 0.30 | Measurement |

(*continued*)

Geosphere, published online on 12 January 2012 as doi:10.1130/GES00534.1



TABLE 3. SOURCE-SIDE SPLITTING MEASUREMENTS (*continued*)

| Station | Distance (°) | Azimuth (°) | Φ (°) | δt (s) | Result |
|---|---|---|---|---|---|
| | | **04 December 2002 (02338)** (*continued*) | | | |
| KONO | 70.9 | 327.6 | 60 ± 23 | — | Null |
| KWP | 63.7 | 316.5 | –13 ± 8 | 3.05 ± 0.80 | Measurement |
| MA2 | 56.6 | 30.5 | –52 ± 9 | 2.85 ± 0.22 | Measurement |
| MDJ | 38.5 | 41.3 | 61 ± 23 | — | Null |
| MORC | 67.1 | 316.7 | 52 ± 23 | — | Null, corrected |
| NWAO | 56.4 | 157.0 | 69 ± 23 | — | Null |
| RGN | 69.3 | 322.0 | 56 ± 7 | — | Null |
| RUE | 69.2 | 319.8 | 75 ± 23 | — | Null |
| SANT | 72.6 | 316.3 | 45 ± 23 | — | Null |
| SUW | 63.6 | 321.4 | 45 ± 23 | — | Null |
| TIXI | 55.9 | 12.5 | 7 ± 9 | 3.35 ± 0.58 | Measurement |
| ULN | 30.2 | 16.9 | 31 ± 7 | 4.35 ± 0.45 | Measurement |
| YAK | 49.1 | 21.1 | 82 ± 23 | — | Null |
| YSS | 47.9 | 43.6 | –57 ± 8 | 2.80 ± 0.25 | Measurement |
| | | **29 November 2004 (04344)** | | | |
| EIL | 51.0 | 289.1 | –43 ± 13 | 2.90 ± 0.38 | Measurement |
| ERM | 45.0 | 54.6 | 48 ± 11 | 3.80 ± 0.50 | Measurement |
| IDI | 58.5 | 297.5 | 76 ± 17 | 2.85 ± 0.98 | Measurement |
| MBAR | 64.8 | 256.8 | 10 ± 23 | — | Null, corrected |
| YAK | 44.9 | 23.8 | 83 ± 23 | — | Null, corrected |
| YSS | 45.5 | 47.6 | –50 ± 8 | 2.90 ± 0.38 | Measurement |
| | | **18 September 2005 (05261)** | | | |
| ANTO | 53.6 | 302.4 | 12 ± 23 | — | Null, corrected |
| ARU | 41.2 | 330.1 | 65 ± 14 | — | Null, corrected |
| GRFO | 67.6 | 315.7 | 47 ± 14 | — | Null, corrected |
| ISP | 55.5 | 300.1 | 15 ± 14 | — | Null |
| KEV | 59.4 | 338.0 | 56 ± 23 | — | Null |
| KIV | 46.3 | 308.0 | 48 ± 23 | — | Null |
| KMBO | 61.3 | 254.1 | 11 ± 23 | — | Null |
| KONO | 66.7 | 326.6 | 45 ± 23 | — | Null |
| LSZ | 76.1 | 245.9 | 2 ± 23 | — | Null |
| MA2 | 52.0 | 32.4 | –45 ± 8 | 3.15 ± 0.25 | Measurement |
| MAJO | 38.9 | 61.8 | –39 ± 4 | 3.70 ± 0.20 | Measurement |
| MBAR | 66.8 | 258.0 | 78 ± 23 | — | Null |
| MORC | 63.5 | 315.1 | 57 ± 23 | — | Null, corrected |
| MSEY | 48.1 | 238.1 | 59 ± 23 | — | Null |
| RUE | 65.5 | 318.4 | 41 ± 23 | — | Null |
| STU | 69.1 | 315.1 | 35 ± 22 | — | Null, corrected |
| YAK | 44.1 | 22.8 | 3 ± 16 | — | Null |
| YSS | 44.0 | 47.1 | –17 ± 17 | 3.10 ± 0.78 | Measurement |
| | | **11 May 2006 (06131)** | | | |
| ANTO | 53.9 | 302.2 | 7 ± 23 | — | Null |
| AQU | 68.1 | 308.0 | 8 ± 3 | — | Null |
| BFO | 70.3 | 315.0 | 9 ± 18 | — | Null |
| BNI | 72.2 | 312.0 | 89 ± 23 | — | Null |
| CTAO | 66.6 | 126.2 | 27 ± 23 | — | Null |
| DSB | 77.7 | 322.8 | 19 ± 23 | — | Null |
| ESK | 75.3 | 324.1 | 15 ± 23 | — | Null |
| GRFO | 68.2 | 316.0 | 22 ± 23 | — | Null |
| HIA | 32.8 | 31.4 | 38 ± 17 | — | Null |
| IDI | 60.6 | 298.5 | 76 ± 6 | 2.55 ± 0.35 | Measurement |
| ISP | 55.8 | 300.8 | 2 ± 23 | — | Null, corrected |
| KEV | 50.5 | 338.4 | 31 ± 23 | — | Null |
| KIV | 46.8 | 309.1 | 34 ± 8 | 3.55 ± 0.32 | Measurement |
| KONO | 67.5 | 326.8 | –78 ± 4 | 4.15 ± 0.45 | Measurement |
| KWP | 60.8 | 315.0 | –54 ± 13 | 3.20 ± 0.35 | Measurement |
| LSZ | 75.1 | 245.9 | 87 ± 23 | — | Null |
| MAHO | 75.4 | 307.4 | 14 ± 8 | 2.00 ± 0.80 | Measurement |
| MORC | 64.1 | 315.5 | –89 ± 13 | 2.20 ± 0.60 | Measurement |
| MSEY | 47.0 | 238.7 | 62 ± 4 | — | Null |
| RUE | 66.2 | 318.7 | 44 ± 20 | 2.35 ± 0.70 | Measurement |
| SSB | 73.6 | 312.6 | 38 ± 7 | 2.70 ± 0.28 | Measurement |
| STU | 69.7 | 315.3 | 3 ± 17 | — | Null |
| TRI | 67.2 | 311.5 | 8 ± 23 | — | Null |
| VSL | 71.8 | 305.8 | 17 ± 23 | — | Null |
| WDD | 68.8 | 300.9 | 2 ± 23 | — | Null, corrected |

coaxial finite strain also typically yields more complicated anisotropic fabrics (Tommasi et al., 1999; Kaminski and Ribe, 2001; Blackman and Kendall, 2002).

The asthenosphere beneath the Arakan slab was likely thoroughly devolatilized during formation of the Indian lithosphere by ridge processes, and the asthenospheric channel beneath the subducted Indian lithosphere is therefore unlikely to include significant water. Although slab dewatering fluids may hydrate the suprasubduction mantle wedge and modify LPO (Jung and Karato, 2001; Bostock et al., 2002; Karato, 2003; Jung et al., 2006; Abt and Fischer, 2008), the mantle beneath the slab is unlikely to have been affected. Also, slow-velocity anomalies visible in the tomographic study of Li et al. (2008) are modest (1% slow) and inconsistent with presence of partial melt beneath the Arakan slab. Thus, a large majority of the shear-wave splitting results at this subduction zone can be linked to A-type anisotropy. Some ray paths (see below) do sample the deeper mantle wedge region, where the increased likelihood of hydration and partial melt fraction make the B-type fabric a potential alternative (e.g., Abt and Fischer., 2008). However, Kneller et al. (2008) show that the conditions for development of B-type anisotropic fabrics (high stress, high water content, and low temperature) are restricted to the shallow mantle wedge region, and so for all downgoing *S* waves used in this study that do not sample the shallow suprasubduction mantle wedge (see below), we adopt the *a*-axis olivine LPO model for interpretations.

### Homogeneous Anisotropy Models

The sampling of the Arakan–Triple Junction region upper mantle achieved, given the locations of the source events and receiver stations, is heterogeneous, but still dense enough in several quadrants for quite a few of the events (see Fig. 10) to rule out interpretations of the observed splitting variations that invoke homogeneous plunging anisotropies. For example, neglecting the strong along-strike component of plate boundary zone motion discernible in both the earthquake focal mechanisms (Figs. 4–6; see also Le Dain et al., 1984; Ni et al., 1989; Stork et al., 2008) and the GPS results for the area (Socquet et al., 2006; Simons et al., 2007), a potential explanation for the variation in source-side *S* splitting results visible in Figure 11 is a single, regionally homogeneous anisotropic symmetry that plunges eastward in the Arakan slab dip direction, as might be produced by 2-D entrained upper-mantle flow at the subduction zone. Upper-mantle fabrics with this orientation

Geosphere, published online on 12 January 2012 as doi:10.1130/GES00534.1



should yield largely N-S–trending fast shear polarizations both west and east of the Arakan slab (Crampin and Booth, 1985; Chevrot and van der Hilst, 2003), which pattern is considerably simpler than that observed, both for individual events and all the events in aggregate.

## Shear-Wave Splitting and Arakan Slab Segmentation

Figure 11, a compilation of all the source-side splitting results of this study, shows that the various source events, which differ in focal mechanism and often in depth, yield shear-wave splitting measurements that are largely consistent with respect to the upper-mantle volumes sampled by *S* waves traveling similar source-receiver travel paths. For example, splitting fast polarizations observed to the east of the northern Arakan slab segment trend NNW-SSE with delay times near 3 s, although the *S* waves derive from no less than six source events, and were recorded at receiver stations with distinct station anisotropy (see Tables 2 and 3). Similar consistency of results is observed for splitting measurements from groups of events sampling other portions of the Arakan slab–Triple Junction region. Potential fast and slow axes of observed splitting nulls also often display similar consistency (Fig. 12), pointing to the presence of similar anisotropic fabrics within these disparate regions around the Arakan slab, although the anisotropic fabrics appear to vary from region to region around the slab and vicinity.

The distinct sampling of the source-side shear-wave splitting can be seen in the theoretical ray paths of *S* waves from the source events to the receiver stations used to make the measurements (Fig. 13). Shear-wave velocities within a Cartesian model volume were assigned based on published variations from a velocity model for the area (Li et al., 2008), which allowed construction of an Arakan slab anomaly 1% higher in velocity than surroundings. Rays were traced along event-station azimuths from the event hypocenters down to 900 km depth. Given the periods of the *S* waves used (10 s, minimum) and the source-receiver distances, which imply sensitivity to structure off the theoretical ray path (Zhao et al., 2000), the ray tracing is meant to show simply that despite such concerns the rays do largely sample distinct regions azimuthally around the individual sources. Thus, averaging the splitting results, for example, would be unwarranted, and, given the scale of geologic heterogeneity visible at the surface, and implied at upper-mantle depths, the fact of variations in observed splitting is unsurprising.

Anisotropic fabrics related to India's northward motion and along-strike shear within the

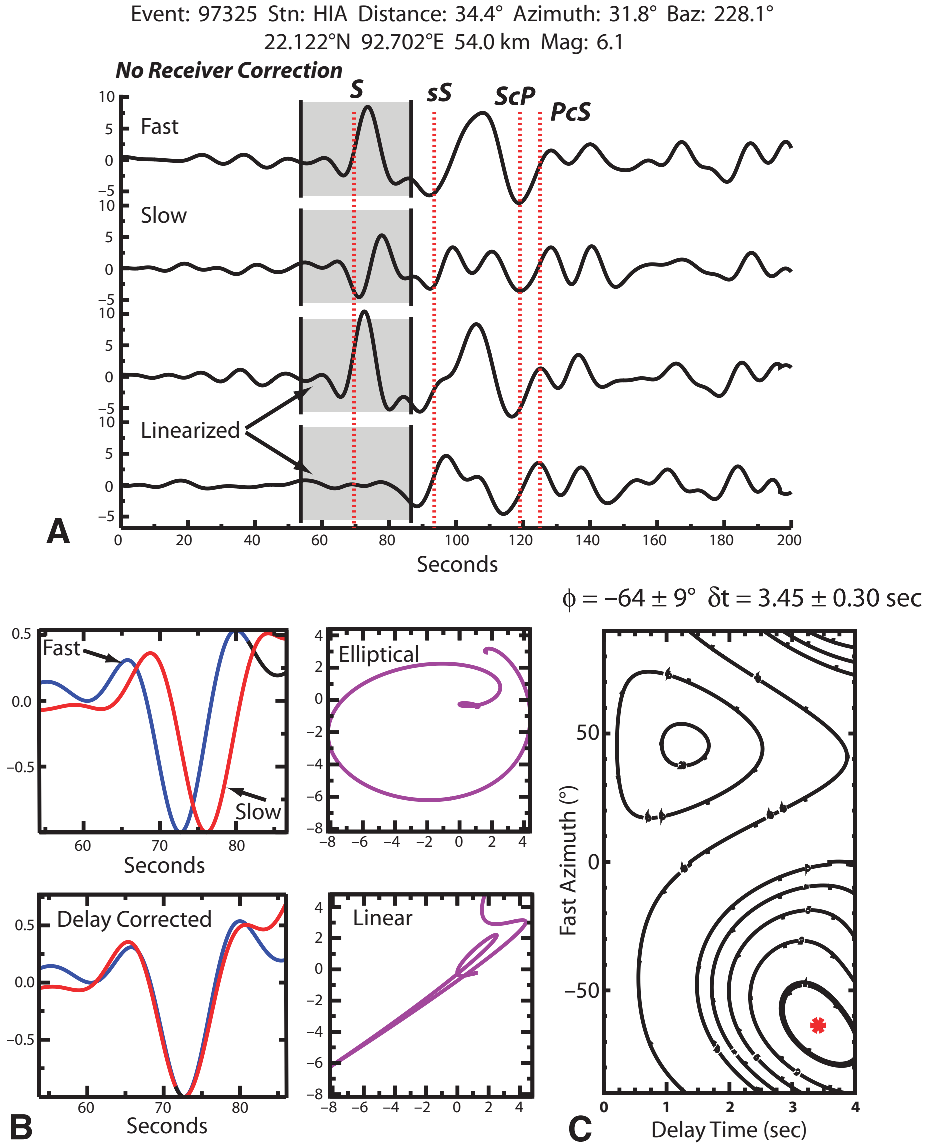


**Figure 9** (*on this and following page*). **(A–C) Example of source-side splitting measurement. (A–C) for measurement uncorrected for receiver-side splitting. (A) Seismograms of event 97325 at station HIA (China). *S* wave in the measurement window (heavy vertical black lines) clearly separated from *sS*. *S* wave rotated to fast-slow component frame (top two traces), and corrected for splitting (bottom two traces). Linearization clearly minimizes energy on seismogram component corresponding to the minimum eigenvalue of the polarization matrix (bottom trace). (B) Top two panels are waveforms (left) and particle motions (right) in fast-slow component frame prior to correction for splitting delay; note good waveform correspondence between fast and slow waves and elliptical particle motion. Bottom two panels show waveforms and particle motions after correction for splitting delay; note linear particle motion after correction (right). (C) Contour of energy on the minimum eigenvalue of the polarization matrix component grid search for all azimuths (vertical axis) and splitting delays from 0 to 4 s (horizontal axis). Best splitting fast azimuth and delay time marked by red star; double contour bounds the 95% confidence limit for this measurement.**

Geosphere, published online on 12 January 2012 as doi:10.1130/GES00534.1



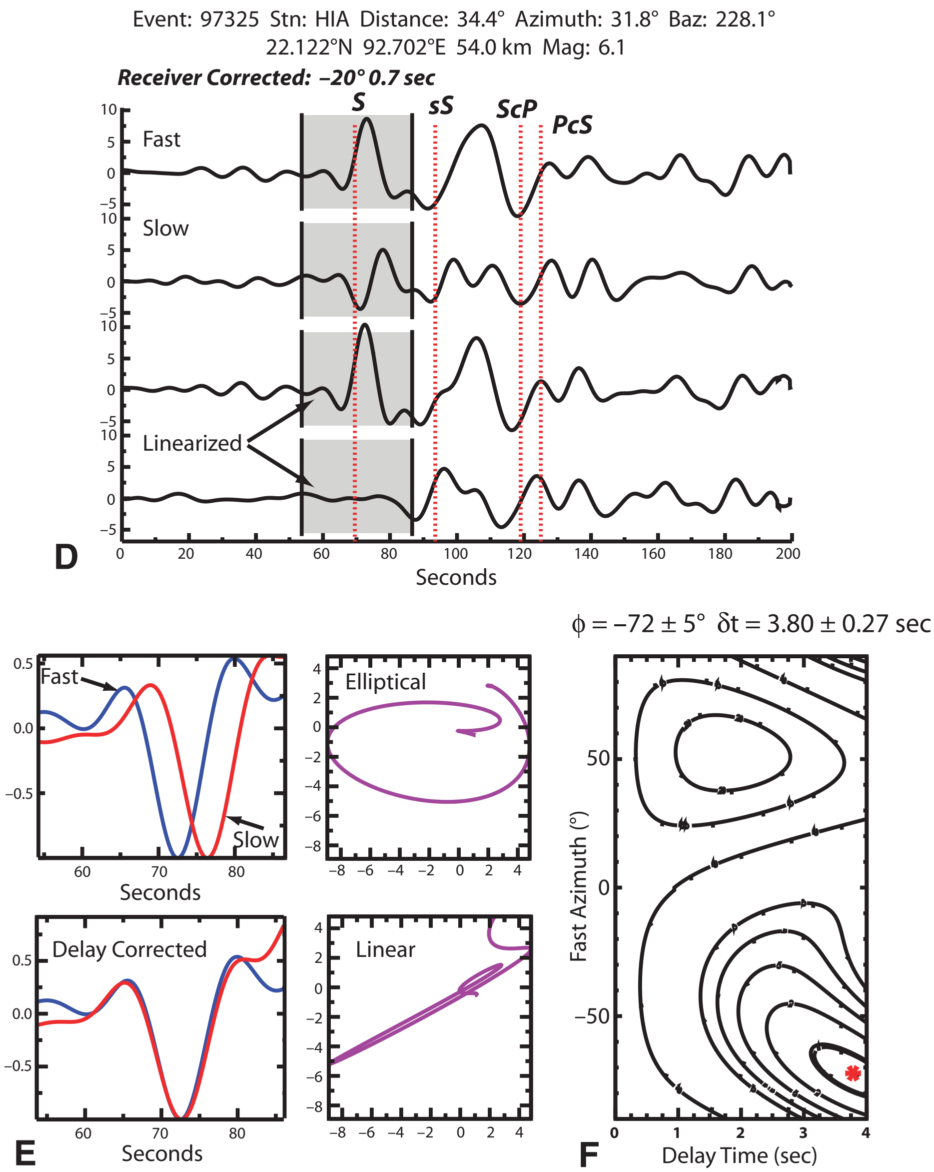


**Figure 9 (*continued*). (D–F) Example of source-side splitting measurement. (D–F) for measurement corrected for receiver-side splitting. (D) Seismograms of event 97325 at station HIA (China). *S* wave in the measurement window (heavy vertical black lines) clearly separated from *sS*. *S* wave rotated to fast-slow component frame (top two traces), and corrected for splitting (bottom two traces). Linearization clearly minimizes energy on seismogram component corresponding to the minimum eigenvalue of the polarization matrix (bottom trace). (E) Top two panels are waveforms (left) and particle motions (right) in fast-slow component frame prior to correction for splitting delay; note good waveform correspondence between fast and slow waves and elliptical particle motion. Bottom two panels show waveforms and particle motions after correction for splitting delay; note linear particle motion after correction (right). (F) Contour of energy on the minimum eigenvalue of the polarization matrix component grid search for all azimuths (vertical axis) and splitting delays from 0 to 4 s (horizontal axis). Best splitting fast azimuth and delay time marked by red star; double contour bounds the 95% confidence limit for this measurement. Note that splitting fast azimuth must be corrected for mirror image projection at surface due to wave path bottoming ($phi_{src}$).**

**Figure 10 (*on following four pages*). Source-side splitting measurements for each event: hypocentral depths and event year and Julian Day in YYJJJ format shown, lower left. Heavy black lines are the three Arakan slab segments. Thin blue lines mark surface-projected ray paths for each event-receiver station pair, down to a depth of 400 km. Focal mechanisms for each event also shown; source: U.S. Geological Survey National Earthquake Information Center. Purple lines show splitting fast trends, corrected for receiver station splitting, and plotted at the surface projection of the point along the event-receiver ray path at 200 km depth. Thin gray crosses show two possible fast shear trends for observed null splitting. Stars are event epicenters, which differ in some cases from centroid locations.**

wide India-Sundaland plate boundary zone can thus be inferred to exist along ray paths that sample the upper-mantle volume west of the slab between ~20°N and south of Shillong Plateau, particularly west of ~94°E longitude (see Fig. 13). Note however that a subset of splitting fast trends spanning the full N-S extent of the western study region appears to be parallel to the Arakan subduction zone strike (e.g., main trace of the high topography of the Indo-Burman ranges, Fig. 1). These observations derive from ray paths that sample a central region—here termed the internal zone—between the more E-W fast splits of the Shillong Plateau group (see below), and a group of splitting observations with NW-SE fast trends that sample the region proximal to the bottom surfaces of the northern two Arakan slab segments. Overall, the internal zone measurements follow a pattern such that the general trend of fast shear south of 22°N is slightly NNW, but north of that latitude the mean trend of this splitting subset is NNE, just as the arcuate subduction zone changes strike from NNW in the south to NNE in the north (Fig. 11).

The basic pattern of splitting west of the Arakan slab is disrupted or modulated near, and just south of, the Shillong Plateau, from ~24° to 25.5°N, where fast splitting axes trend ENE and E-W, similar to the strike of the Plateau itself (E-W) and perhaps indicating interaction of, or transition between, two upper-mantle anisotropic fabrics: N-S–striking fabrics due to India-Sundaland shear, and E-W flattening fabrics developed orthogonal to the N-S compression of the India-Asia collision. Also, projecting southwards along strike of the Arakan slab near the southern limit of deeper slab

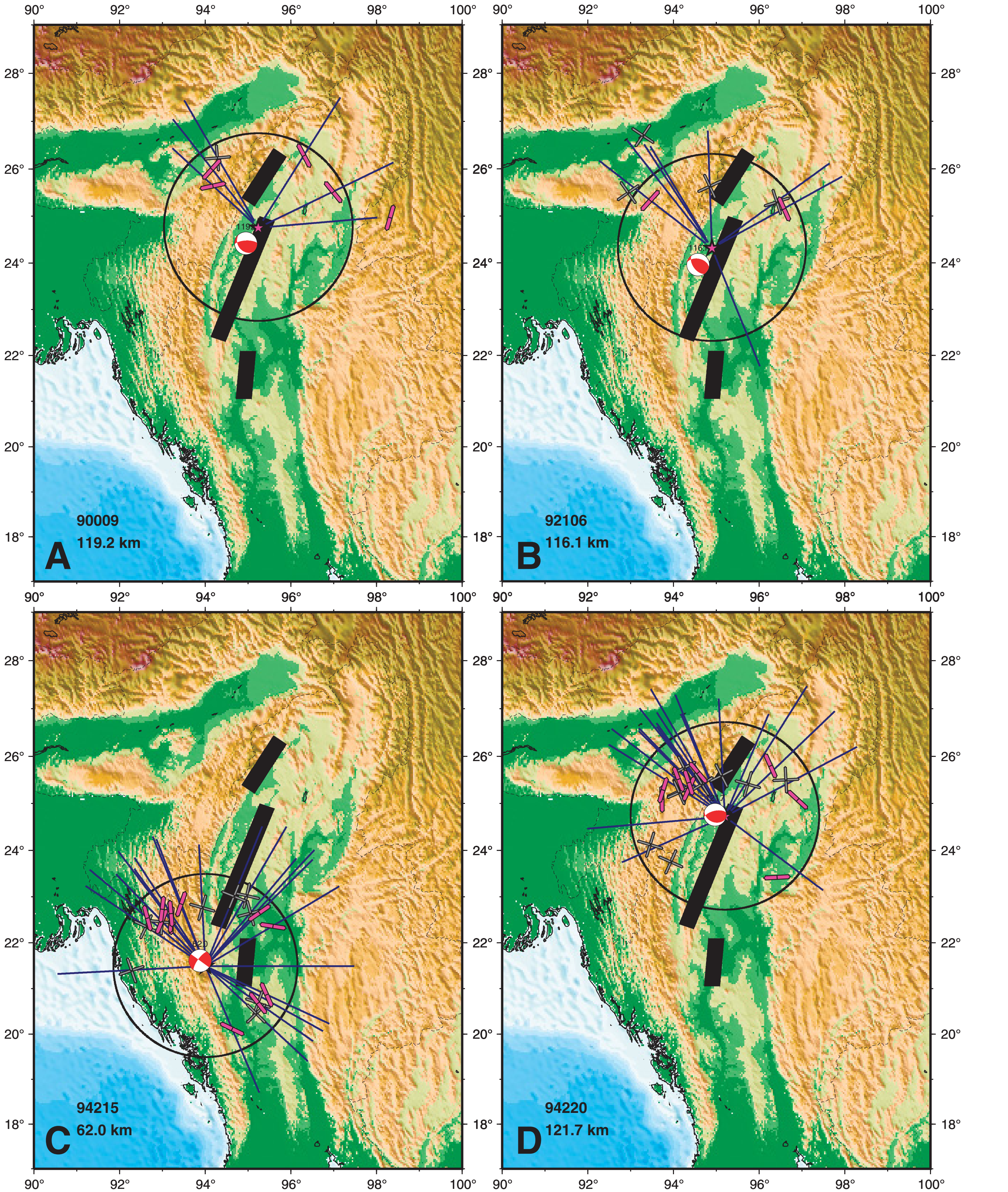
90009
119.2 km
A
92106
116.1 km
B
94215
62.0 km
C
94220
121.7 km
D
90°
92°
94°
96°
98°
100°
18°
20°
22°
24°
26°
28°

**Figure 10.**

Geosphere, published online on 12 January 2012 as doi:10.1130/GES00534.1



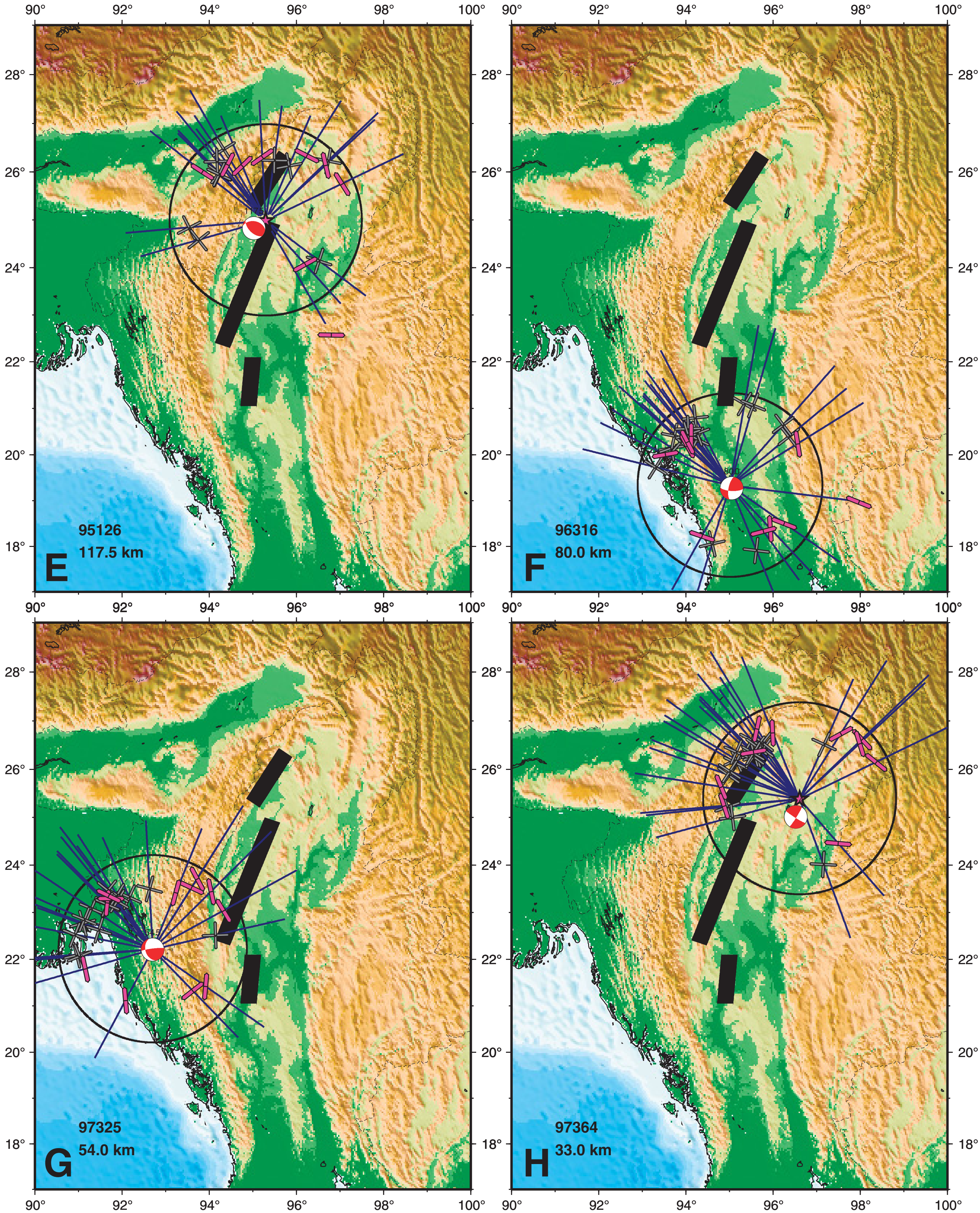


**Figure 10 (*continued*).**

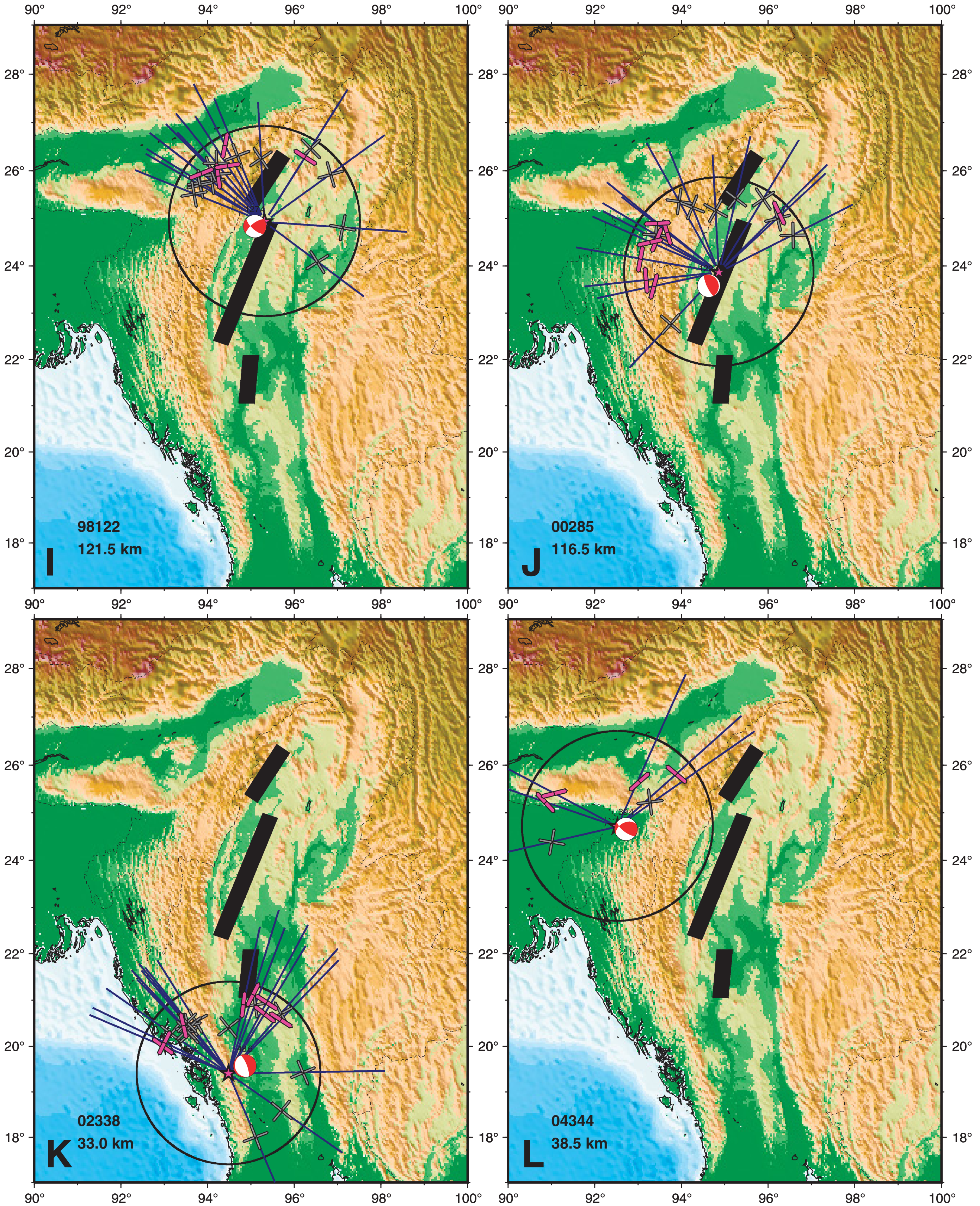


**Figure 10 (*continued*).**

Geosphere, published online on 12 January 2012 as doi:10.1130/GES00534.1



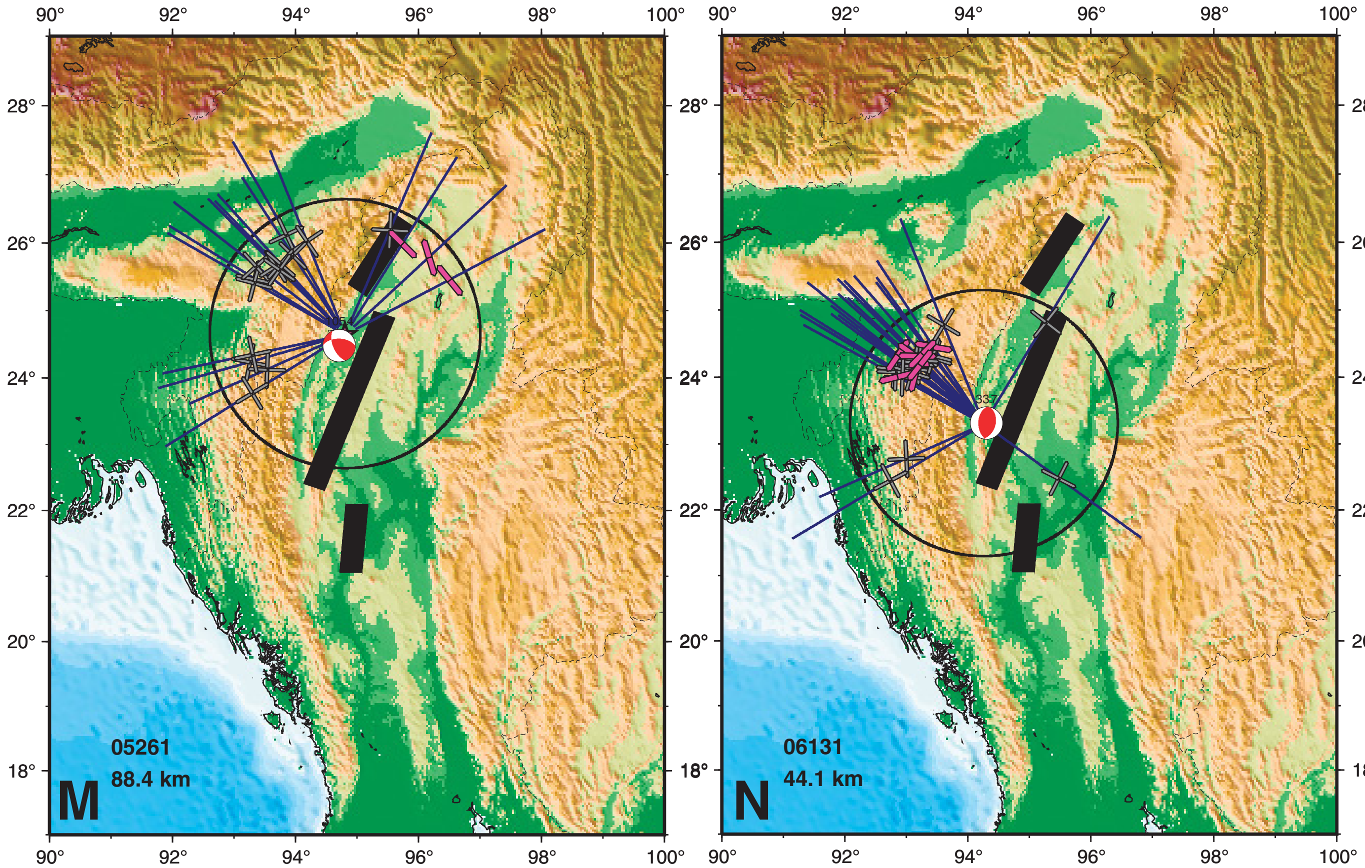


**Figure 10 (*continued*).**

seismicity, south of 20°N, shear-wave splitting fast axes trend E-W, possibly indicating that upper-mantle flows around the southern slab edge. If so, then subducted Indian lithosphere is not continuous between the southern seismicity of the Arakan slab and the northernmost intermediate depth seismicity of the Andaman subduction segment, an issue not resolved by available tomography (Li et al., 2008).

For ray paths sampling to the east of the Arakan slab, the results are divisible into three groups: north of 24.3°N, splitting fast axes trend NW-SE to NNW-SSE; in a central region (22°–24.3°N), fast axes are E-W; and south of 21°N, predominantly NW-SE fast axes are observed. The northern group of splitting fast axes appears to be part of a limb of upper-mantle flow around the northern edge of the northern Arakan slab segment (Fig. 11). The central group may be related to upper-mantle flow through the gap between the northern and southern Arakan slab segments (Fig. 11), and may also be part of the larger-scale flow field beneath the Shan Plateau (see below). The southern group of measurements east of the Arakan slab appears to be consistent with upper-mantle flow around the southern terminus of the Arakan slab.

## Shear-Wave Splitting and Upper-Mantle Flow

The source-side splitting measurements shown in Figure 11 are consistent with observations of *SK(K)S*/*PKS* splitting made at nearby seismic stations (Fig. 14) (Vinnik et al., 1992; Lev et al., 2006; Singh et al., 2006, 2007; Huang et al., 2007). In NE India, station fast shear-wave polarizations generally trend E-W, except near the western Shillong Plateau, where fast axes trend ENE-WSW (Singh et al., 2006, 2007). To the east, splitting fast directions trend NNW-SSE, north of ~26°N, before abruptly changing to E-W trends south of that latitude (data shown from Lev et al., 2006; and Huang et al., 2007; but see also Flesch et al., 2005; Sol et al., 2007; Wang et al., 2008). At station CHTO, at Chiang Mai, Thailand, in the southeast of the study region, the fast shear trend is also nearly E-W (Vinnik et al., 1992). In almost all cases, adjacent source-side and station splitting measurements are similar in fast polarization direction (Fig. 14). Thus, the differing travel paths (upgoing and traversing the entire anisotropic upper mantle for *SK(K)S*/*PKS*, and downgoing from the individual event hypocenters for *S*) and methods used to measure splitting in these studies (those in this study corrected for receiver station splitting, which is unnecessary for the others) yield the same results.

East of 96°E, E-W fast source-side and station splits generally parallel important surface structures of the western Shan Plateau (Fig. 14), i.e., the long, smoothly linear curving valleys visible in Figure 14. These valleys are geomorphic expressions of a series of near-parallel, sinistral strike-slip faults, the Mengxing, Mae Chan, Nam Ma (and other) faults (Shen et al., 2005; Simons et al., 2007). The faults are seismically active, with fairly frequent left-lateral earthquake focal mechanisms (Fig. 4), and appear to form the westernmost part of the Indochina-wide surface expression of upper-mantle flow around the East Himalayan syntaxis (e.g., Sol et al., 2007; Wang et al., 2008). Note that such flow would then comprise a complete reversal of direction, from eastward flow beneath Tibet north of the syntaxis to westward flow into the suprasubduction mantle wedge above the Arakan slab in Myanmar. It does not seem at all coincidental that these Shan Plateau structures and the generally E-W shear-wave splitting both develop at ~26°N latitude. In fact, this latitude appears to mark an

Geosphere, published online on 12 January 2012 as doi:10.1130/GES00534.1



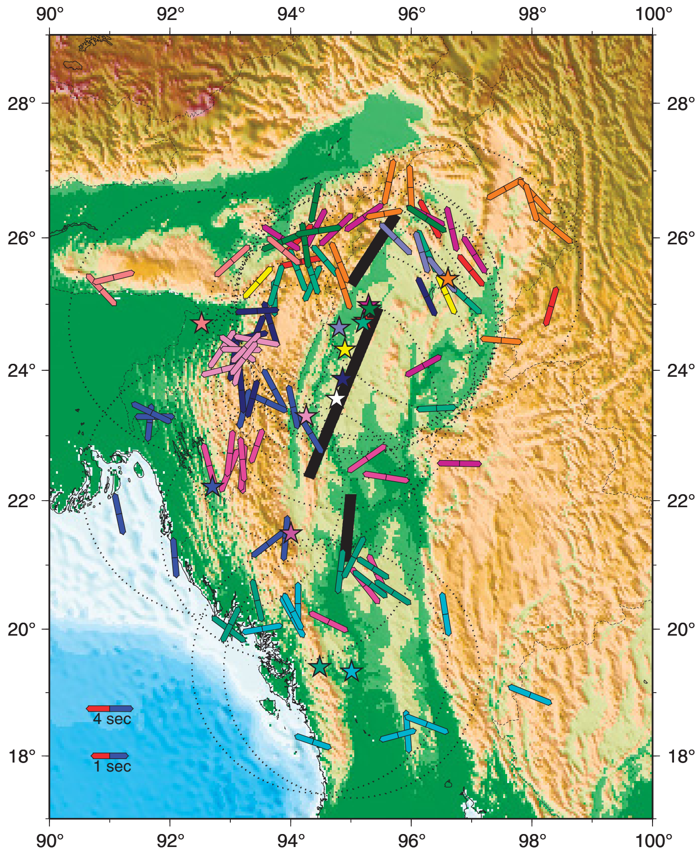


**Figure 11. Source-side splitting measurements for all study events. Epicenters marked by colored stars, and fast shear trends (plotted at surface projection of 200 km point along ray path) colored same as source event star. Dotted circles for each event mark ~200 km radius source hemisphere for reference. Delay times as per key, lower left.**

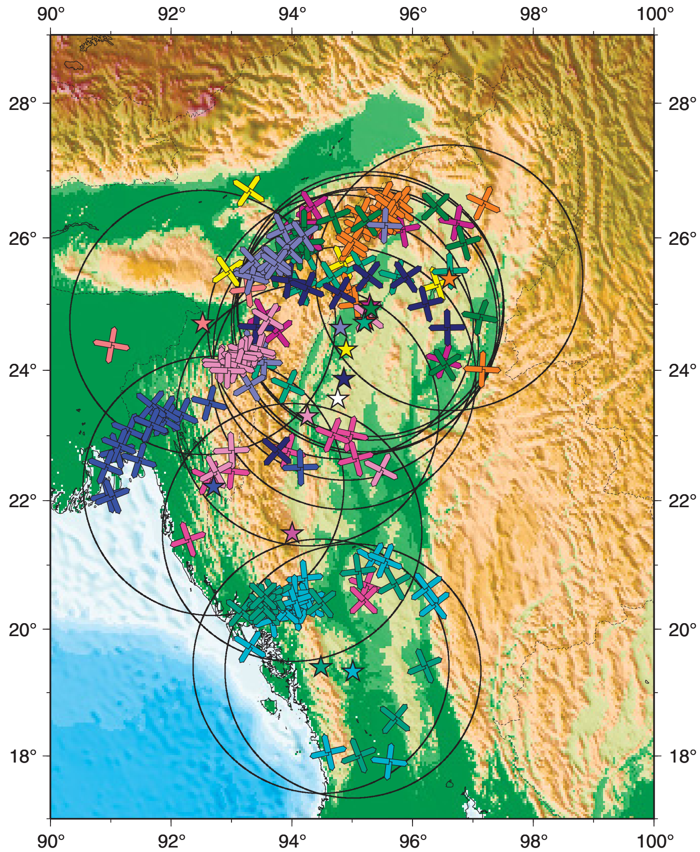


**Figure 12. All null splitting observations. Epicenters and potential splitting fast axes color coded as in Figure 11. Two-hundred km source-sphere projections shown as black circles.**

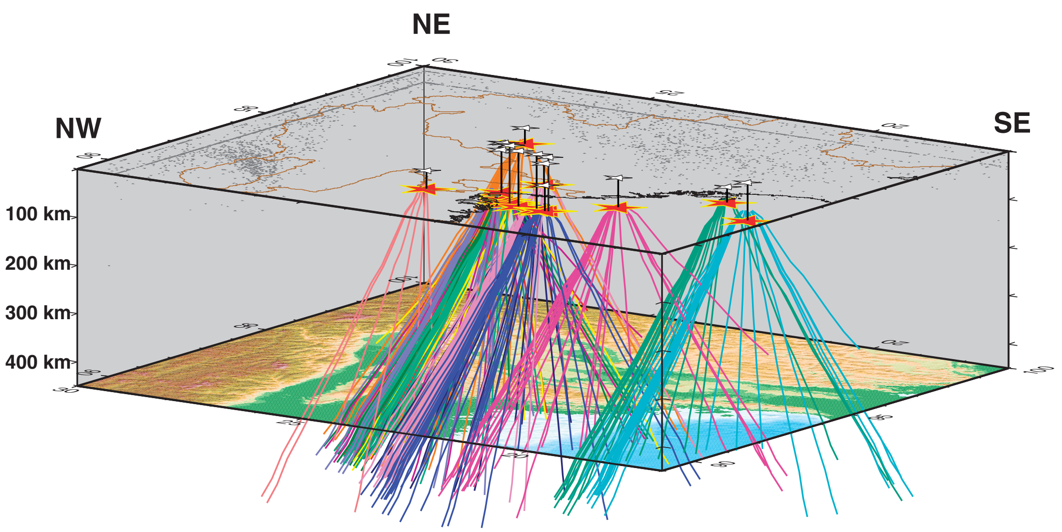


**Figure 13. Block diagram view of source-receiver ray paths from ray tracing, discussed in text. Rays for each event color coded. Red stars mark hypocenters. Topography plotted at box bottom for reference. View from the SW looking NE.**

Geosphere, published online on 12 January 2012 as doi:10.1130/GES00534.1



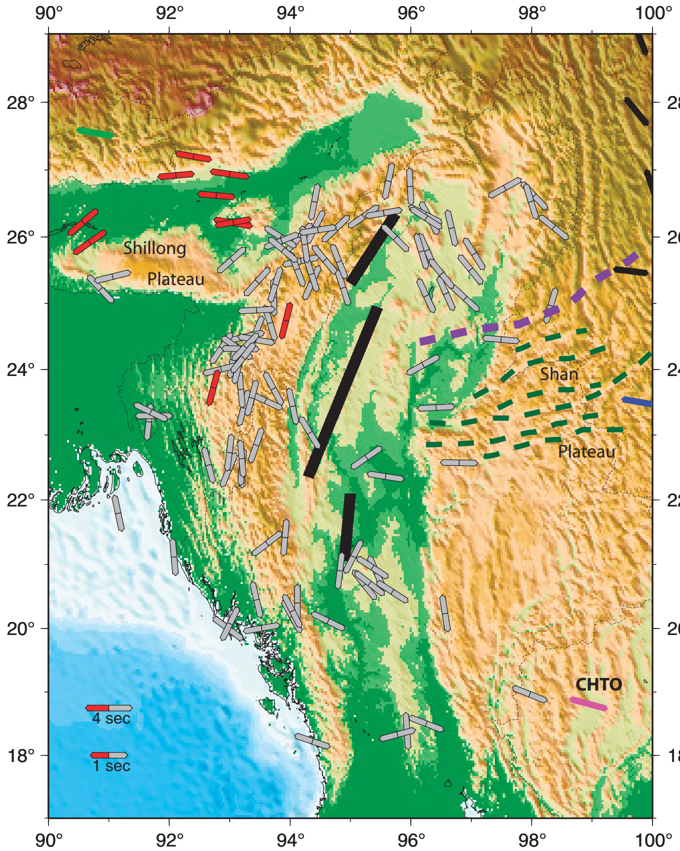


**Figure 14. Source-side (gray) and station (colored) splitting results. Red bars: splits from Singh et al. (2006); light green: splits from Singh et al. (2007). Black bars: splits from Lev et al. (2006); blue bars: splits from Huang et al. (2007). CHTO split from Vinnik et al. (1992). Dark-green dashed lines mark Shan Plateau faults; purple dashed line is approximate northern boundary of E-W fast splitting.**

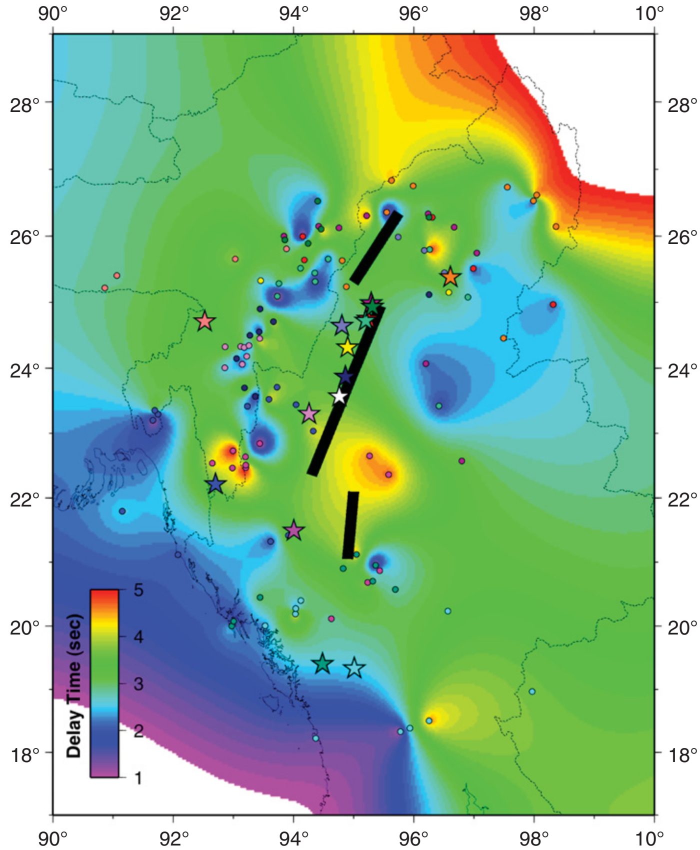


**Figure 15. Contoured splitting delay times, as per key lower left. Heavy red lines mark Arakan slab segments. Colored circles are splitting measurement surface projections contributing delay time estimates to the contouring. Stars mark event epicenters, colored same as corresponding splitting delay time circles.**

important structural boundary not only at the surface, but also at depth: the offset between the northern and central Arakan slab segments, the Shillong Plateau, and the northern limit of Chittagong-Tripura fold belt structures all lie approximately at this latitude (Fig. 14), and are almost certainly expressions of the combined upper-mantle flow and Arakan slab deformation due to the collisional tectonics of the syntaxis. The slab appears to act as a strong strut, now deforming, which indents Asia at the syntaxis efficiently, and which modulates both the larger-scale upper-mantle flow field on the Asia side of the collision zone (Shen et al., 2005; Lev et al., 2006; Sol et al., 2007; Wang et al., 2008), and also the smaller-scale fabrics of the Arakan slab segments, where flow both below and above the slab segments appears to be affected.

Upper-mantle fabric development should be strongest where coaxial finite deformation is strongest (e.g., Ramsay and Lisle, 2000). Assuming observed splitting delay times are a proxy for anisotropic fabric strength (e.g., Gueguen and Nicolas, 1980; Nicolas and Christensen, 1987), contouring of the delay times could potentially reveal regions where upper-mantle flow is strongest or most coherent. Figure 15 shows the results of such contouring: delay times—and upper-mantle flow fabric strength?—appear to be greatest near the East Himalayan syntaxis, in the SE portion of the study region, and also near the offset between the central and southern Arakan slab segments. Secondary clusters of high delay times occur around the northern edge of the northern Arakan slab segment, near the eastern Shillong Plateau, and as an isolated pocket beneath the central Chittagong-Tripura fold belt. Strong fabric development due to upper-mantle flow around the tightly curved northern edge of the Arakan slab and also around the syntaxis itself would not be surprising. Flow through any kind of narrow channel, such as perhaps exists between the central and southern Arakan slab segments, is also commensurate with observations from fluid dynamics (e.g., Schlichting and Gersten, 2000). The causes of localized high delay times in the southeast of the study area and beneath the fold belt are unclear.

### Scale of Upper-Mantle Flow

The distinct anisotropic volumes delineated by the shear-wave splitting observations outlined above are shown schematically in Figure 16. Several conclusions can be drawn: (1) The source events occurred at depths of 50–100 km, and sampled anisotropic fabrics from those depths down to the top of the transition zone. The Arakan slab segments extend from near the surface (Ni et al., 1989; Rao and Kalpna, 2005; Stork et al., 2008) to the top of the transition zone (Li et al., 2008). And finally, the geology of the syntaxis region, NE India, Yunnan, and the Shan Plateau can be related to the splitting results, both source-side observations of

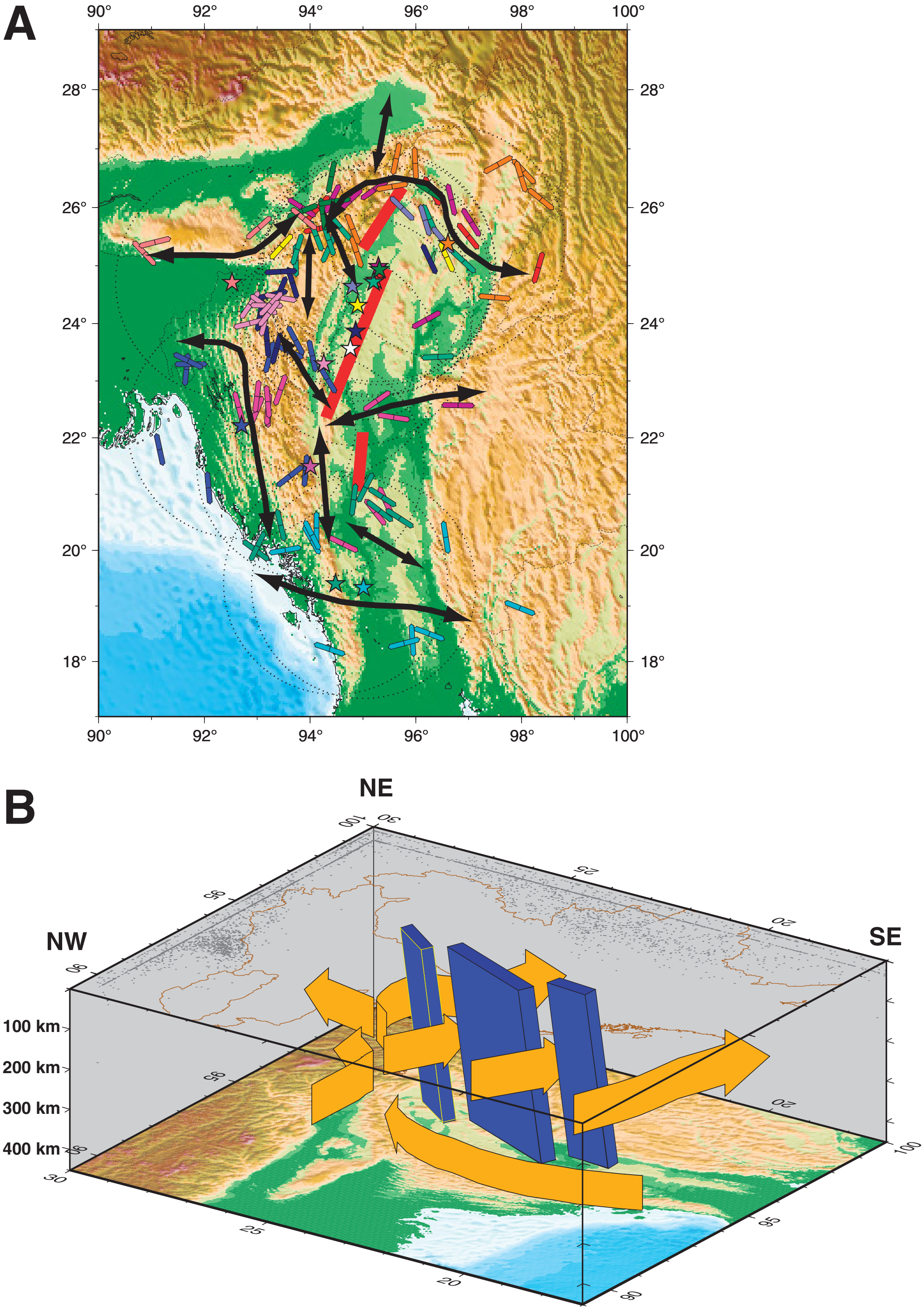


**Figure 16. (A) Source-side splitting measurements as shown in Figure 11, with interpreted domainal fabric directions superposed (two-headed black arrows). Arakan slab segments marked by heavy red lines. Event epicenters are colored stars. Dotted circles as per Figure 11. (B) Upper mantle flow (large orange arrows) in vicinity of subducted Arakan lithosphere (three en-echelon offset segments represented by east-dipping blue slabs). Flow directions conform to interpreted domainal upper mantle fabrics delineated by source side splitting measurements as shown in Figure 11.**

this study and station splitting published by others. These observations all imply that the upper-mantle flow field extends from the surface perhaps to the top of the transition zone. (2) Laterally, there seem to be two scales of anisotropic fabric and flow: a smaller-scale flow field, defined by source-side splitting observations around the Arakan slab segments, varies on the order of 50–75 km laterally. A larger-scale structure of anisotropic upper-mantle fabrics is also clearly developed and appears to be determined by the regional form of the India-Asia collision, i.e., the large-scale material flow around the east Himalayan syntaxis. (3) The transitions between these two scales of the upper-mantle flow field, and between the domains of the smaller-scale Arakan slab fabrics, appear to be rather sharp. If so, then strain partitioning of upper-mantle deformation would appear to occur: the transition from the generally E-W flow field of the Himalayas, NE India,

Geosphere, published online on 12 January 2012 as doi:10.1130/GES00534.1



and the Shillong Plateau (Singh et al., 2006, 2007) to the slab-parallel fabrics of the Arakan internal zone, appears to be abrupt (Figs. 11, 16; see Fig. 13 for sampling). An abrupt transition between the flow fields suggests the presence of domainal deformations (in the structural geology sense) bounded by much narrower zones of stronger shear, and perhaps even ductile faults in the upper mantle. One implication of the existence of volumes of generally homogeneous coaxial finite strain bounded by high-strain shear zones is that large-scale deformation may not proceed similarly to the deformation of viscous continua.

### An Olivine B-Axis Anisotropic Fabric?

An interesting question is whether the mantle wedge above the Arakan slab could actually be characterized by predominantly *b*-axis anisotropic fabrics, with concomitant orientation of flow in the suprasubduction wedge? If so, the mantle wedge flow field would then actually be N-S, consistent with generally N-S shear between northward-propagating India and Indochina extruding southeastwards, but, as indicated by many splitting observations, this flow field would then extend to at least 102°E (Lev et al., 2006; Sol et al., 2007; Wang et al., 2008), far to the east of the region normally considered to be upper-mantle wedge. If the flow field were actually this wide (some 600 km) and anisotropic *b*-axis fabrics predominated throughout, some as yet unidentified mechanism for hydrating or partially melting the upper mantle far beyond the normal width of the Arakan upper-mantle wedge would appear to be required (e.g., Kneller et al., 2008). Note that if the shallow Arakan slab (the closest known source of hydrated material) is the source of the water, the hydration process would have to transport material effectively across the dominant N-S mantle fabrics organized by upper-mantle flow. Alternatively, dewatering of the Indian lithosphere lying at the top of the transition zone (Li et al., 2008) could potentially hydrate the upper mantle from below without entailing cross-flow material transport (see also Van der Lee et al., 2008). If we assume *b*-axis fabrics have formed due to presence of partial melt, then apparent E-W fast splitting in the central part of the Arakan upper-mantle wedge would actually imply N-S flow fabrics, cutting across the E-W grain of surface structures of the Shan Plateau. Note that such flow fabrics would be inconsistent with 2-D mantle wedge corner flow, and would presumably also imply an abnormally wide mantle wedge region.

Finally, simple asthenospheric flow (e.g., Vinnik et al., 1989a, 1989b) could also be invoked to explain generally E-W splitting fast axes beneath eastern Myanmar and Indochina south of 26°N, as observed in this study and those of Lev et al. (2006), Huang et al. (2007), Sol et al. (2007), and Wang et al. (2008). If basal shear beneath a generally east-moving Sundaland (relative to stable Eurasia; Simons et al., 2007) organizes upper-mantle deformation fabrics, then one would expect the asthenospheric channel to show generally E-W fast splitting trends. Such basal shear would extend beneath almost all of Indochina, consistent with GPS results (Simons et al., 2007), and could explain the great eastward extent of the splitting observations—far beyond the normal width of suprasubduction upper-mantle wedge—without requiring either *b*-axis anisotropic fabrics or ad hoc mechanisms for hydrating or partially melting the upper-mantle wedge and beyond.

## CONCLUSIONS

Shear-wave splitting of *S* waves from earthquakes in the Arakan slab is consistent with strong upper-mantle anisotropy in the India-Asia-Sundaland triple junction region. The Arakan slab is dismembered into three segments, defined by high-precision relocations of intermediate earthquake, and approximately E-W offsets of these hypocenters at two locations define a left-stepping en echelon structure. *S* waves from earthquakes within the three segments and surroundings are split systematically, and, corrected for receiver-side splitting, fast shear trends are predominantly trench-parallel beneath the east-dipping slab segments; are more nearly trench-normal on the Sundaland (east) side of the Arakan lithosphere; parallel the southern ~E-W gap between Arakan slab segments; and turn sharply around the extreme northern and southern edges of subducted Arakan lithosphere. Source-side shear-wave splitting beneath India is consistent with ~E-W–trending fast shear polarizations of *SK(K)S* splitting in northeastern India. The general pattern of both surface site velocities from GPS and upper-mantle flow is consistent with material flow around the eastern Himalayan syntaxis into the mantle wedge above the Arakan slab, and around the northern edge of the Arakan slab. The upper mantle may also flow through the gap between the central and southern Arakan slab segments, and around the apparent southern edge of the Arakan slab.

#### ACKNOWLEDGMENTS

The shear-wave splitting database published online by the group at the Laboratoire de Tectonophysique, Université de Montpellier II, was indispensable in finding suitable stations for receiver-side correction (see http://www.gm.univ-montp2.fr/splitting/DB/). I am grateful to Martin Flower, Mian Liu, Victor Mocanu, Suzan van der Lee, and Liz Widom for many stimulating discussions of Sundaland tectonics and geochemistry. Associate Editor Craig Jones and two anonymous reviewers made very useful suggestions for improving the manuscript. All data used in this study were downloaded from the IRIS Data Management Center.

#### REFERENCES CITED

Abt, D.L., and Fischer, K.M., 2008, Resolving three-dimensional anisotropic structure with shear-wave splitting tomography: Geophysical Journal International, v. 173, p. 859–886, doi:10.1111/j.1365-246X.2008.03757.x.

Acharyya, S.K., 2007, Collisional emplacement history of the Naga-Andaman ophiolites and the position of the eastern Indian suture: Journal of Asian Earth Sciences, v. 29, p. 229–242, doi:10.1016/j.jseaes.2006.03.003.

Alam, M., Alam, M.M., Curray, J.R., Chowdhury, M.L.R., and Gani, M.R., 2003, An overview of the sedimentary geology of the Bengal Basin in relation to the regional tectonics framework and basin-fill history: Sedimentary Geology, v. 155, p. 177–208.

Ayele, A., Stuart, G., and Kendall, J.-M., 2004, Insights into rifting from shear-wave splitting and receiver functions: An example from Ethiopia: Geophysical Journal International, v. 157, p. 354–362, doi:10.1111/j.1365-246X.2004.02206.x.

Babuska, V., Plomerova, J., Vecsey, L., Granet, M., and Achauer, U., 2002, Seismic anisotropy of the French Massif Central and predisposition of Cenozoic rifting and volcanism by Variscan suture hidden in the mantle lithosphere: Tectonics, v. 21, doi:10.1029/2001TC901035.

Barruol, G., and Ben Ismail, W., 2001, Upper mantle anisotropy beneath the African IRIS and Geoscope stations: Geophysical Journal International, v. 146, p. 549–561.

Barruol, G., and Russo, R.M., 1996, Shear-wave splitting at IRIS GSN stations: Eos (Transactions, American Geophysical Union), v. 77, Supplement, p. 269.

Barruol, G., and Hoffman, R., 1999, Upper mantle anisotropy beneath the Geoscope stations: Journal of Geophysical Research, v. 104, p. 10,757–10,773, doi:10.1029/1999JB900033.

Beck, R.A., and 14 others, 1995, Stratigraphic evidence for an early collision between northwest India and Asia: Nature, v. 373, p. 55–58, doi:10.1038/373055a0.

Behn, M.D., Conrad, C.P., and Silver, P.G., 2004, Detection of upper mantle flow associated with the African superplume: Earth and Planetary Science Letters, v. 224, p. 259–274, doi:10.1016/j.epsl.2004.05.026.

Ben Ismail, W., and Mainprice, D., 1998, An olivine fabric database: An overview of upper mantle fabrics and seismic anisotropy: Tectonics, v. 296, p, 145–147.

Bilham, R., and England, P., 2001, Plateau "pop-up" in the great 1897 Assam earthquake: Nature, v. 410, p. 806–809, doi:10.1038/35071057.

Bjarnason, I.T., Silver, P.G., Rumpker, G., and Solomon, S.C., 2002, Shear wave splitting across the Iceland hot spot: Results from the ICEMELT experiment: Journal of Geophysical Research, v. 107, p. 2382–2394.

Blackman, D.K., and Kendall, J.-M., 2002, Seismic anisotropy in the upper mantle: 2, Predictions for current plate boundary flow models: Geochemistry Geophysics Geosystems, v. 3, p. 18.

Bostock, M., Hyndman, R.D., Rondenay, S., and Peacock, S.M., 2002, An inverted continental Moho and serpentinization of the forearc mantle: Nature, v. 417, p. 536–538.

Carter, N., Baker, D., and George, R., 1972, Seismic anisotropy, flow and constitution of the upper mantle, *in* Heard, H., Borg, I., Carter, N., and Raleigh, C., eds., Flow and Fracture of Rocks: Washington, D.C., American Geophysical Union Geophysical Monograph 16, p. 167–190.

Chamot-Rooke, N., and Le Pichon, X., 1999, GPS determined eastward Sundaland motion with respect to Eurasia confirmed by earthquake slip vectors at the Sunda and Philippine trenches: Earth and Planetary Science Letters, v. 173, p. 439–455, doi:10.1016/S0012-821X(99)00239-3.

Geosphere, published online on 12 January 2012 as doi:10.1130/GES00534.1




Chevrot, S., and van der Hilst, R., 2003, On the effects of a dipping axis of symmetry on shear wave splitting measurements in a transversely isotropic medium: Geophysical Journal International, v. 152, p. 497–505, doi:10.1046/j.1365-246X.2003.01865.x.

Christensen, N.I., 1984, The magnitude, symmetry, and origin of upper mantle anisotropy based on fabric analyses of ultramafic tectonics: Geophysical Journal of the Royal Astronomical Society, v. 76, p. 89–112.

Clark, M.K., and Bilham, R., 2008, Miocene rise of the Shillong Plateau and the beginning of the end for the eastern Himalaya: Earth and Planetary Science Letters, v. 269, p. 337–351, doi:10.1016/j.epsl.2008.01.045.

Crampin, S., and Booth, D.C., 1985, Shear-wave polarizations near the North Anatolian fault—II. Interpretation in terms of crack-induced anisotropy: Geophysical Journal of the Royal Astronomical Society, v. 83, p. 75–92.

Cummins, P.R., 2007, The potential for giant tsunamigenic earthquakes in the northern Bay of Bengal: Nature, v. 449, p. 75–78, doi:10.1038/nature06088.

Curray, J.R., 2005, Tectonics and history of the Andaman Sea region: Journal of Asian Earth Sciences, v. 25, p. 187–232, doi:10.1016/j.jseaes.2004.09.001.

Dasgupta, S., Mukhopadhyay, M., Battacharya, A., and Jana, T., 2003, The geometry of the Burmese-Andaman subducting lithosphere: Journal of Seismology, v. 7, p. 155–174, doi:10.1023/A:1023520105384.

Deng, J.F., Mo, X.X., Zhao, H.L., Wu, Z.X., Luo, Z.H., and Su, S.G., 2004, A new model for the dynamic evolution of Chinese lithosphere: Continental roots-plume tectonics: Earth-Science Reviews, v. 65, p. 223–275, doi:10.1016/j.earscirev.2003.08.001.

Ekstrom, G., Dziewonski, A., and Nettles, M., 2006, The Global CMT Project: www.globalcmt.org.

Fischer, K.M., and Wiens, D.A., 1996, The depth distribution of mantle anisotropy beneath the Tonga subduction zone: Earth and Planetary Science Letters, v. 142, p. 253–260, doi:10.1016/0012-821X(96)00084-2.

Flesch, L.M., Holt, W.E. Silver, P.G., Stephenson, M., Wang, C.-Y., and Chan, W.W., 2005, Constraining the extent of crust-mantle coupling in central Asia using GPS, geologic and shear wave splitting data: Earth and Planetary Science Letters, v. 238, p. 248–268, doi:10.1016/j.epsl.2005.006.023.

Flower, M.J.F., Tamaki, K., and Hoang, N., 1998, Mantle extrusion: A model for dispersed volcanism and DUPAL-like asthenosphere in east Asia and the western Pacific, *in* Flower, M.F.J., Chung, S.-L., Lee, T.-Y., and Lo C.-H., eds., Mantle Dynamics and Plate Interactions in East Asia: Washington, D.C., American Geophysical Union, Geodynamics Ser. 27, p. 67–88.

Flower, M.F.J., Russo, R.M., Tamaki, K., and Hoang, N., 2001, Mantle contamination and the Izu-Bonin-Mariana (IBM) "high-tide mark": Evidence for mantle extrusion caused by Tethyan closure: Tectonophysics, v. 333, p. 9–34, doi:10.1016/S0040-1951(00)00264-X.

Fouch, M.J., and Fischer, K.M., 1996, Mantle anisotropy beneath northwest Pacific subduction zones: Journal of Geophysical Research, v. 101, p. 15,987–16,002, doi:10.1029/96JB00881.

Garcia, T.M., and Russo, R.M., 2005, Mantle flow beneath the Pacific Basin determined via shear wave splitting: Eos (Transactions, American Geophysical Union), v. 86, no. 52.

Gueguen, Y., and Nicolas, A., 1980, Deformation of mantle rocks: Annual Review of Earth and Planetary Sciences, v. 8, p. 119–144, doi:10.1146/annurev.ea.08.050180.001003.

Guzman-Speziale, M., and Ni, J., 1996, Seismicity and tectonics of the western Sunda Arc, *in* Yin, A., and Harrison, M., eds., The Tectonic Evolution of Asia: New York, Cambridge University Press, p. 63–84.

Hall, S.A., Kendall, J.-M., and van der Baan, M., 2004, Some comments on the effects of lower-mantle anisotropy on *SKS* and *SKKS* phases: Physics of the Earth and Planetary Interiors, v. 146, p. 469–481, doi:10.1016/j.pepi.2004.05.002.

Helffrich, G., Silver, P.G., and Given, H., 1994, Shear wave splitting variations over short spatial scales on continents: Geophysical Journal International, v. 119, p. 561–573, doi:10.1111/j.1365-246X.1994.tb00142.x.

Hess, H.H., 1964, Seismic anisotropy of the uppermost mantle under oceans: Nature, v. 203, p. 629–631, doi:10.1038/203629a0.

Holtzman, B.K., Kohlstedt, D.L., Zimmerman, M.E., Heidelbach, F., Hiraga, T., and Hustoft, J., 2003, Melt segregation and strain partitioning: Implications for seismic anisotropy and mantle flow: Science, v. 301, p. 1227–1230, doi:10.1126/science.1087132.

Huang, Z., Wang, L., Xu, M., Liu, J., Mi, N., and Liu, S., 2007, Shear wave splitting across the Ailao Shan–Red River fault zone, SW China: Geophysical Research Letters, v. 34, doi:10.1029/2007GL031236.

Iidaka, T., and Niu, F., 2001, Mantle and crust anisotropy in the eastern China region inferred from waveform splitting of *SKS* and *PpSms*: Earth, Planets, and Space, v. 53, p. 159–168.

Jade, S., Mukul, M., Bhattacharvya, A.K., Vijavan, M.S.M., Jaganathan, S., Kumar, A., Tiwari, R.P., Kumar, A., Kalita, S., Sahu, S.C., Krishna, A.P., Gupta, S.S., Murthy, M.V.R.L., and Gaur, V.K., 2007, Estimates of interseismic deformation in Northeast India from GPS measurements: Earth and Planetary Science Letters, v. 263, p. 221–234, doi:10.1016/j.epsl.2007.08.031.

Jung, H., and Karato, S., 2001, Water-induced fabric transitions in olivine: Science, v. 293, p. 1460–1464, doi:10.1126/science.1062235.

Jung, H., Katayama, I., Jiang, Z., Hiraga, T., and Karato, S., 2006, Effect of water and stress on the lattice-preferred orientation of olivine: Tectonphysics, v. 421, p. 1–22, doi:10.1016/j.tecto.2006.02.011.

Kaminski, E., and Ribe, N., 2001, A kinematic model for recrystallization and texture development in olivine polycrystals: Earth and Planetary Science Letters, v. 189, p. 253–267, doi:10.1016/S0012-821X(01)00356-9.

Karato, S., 2003, Mapping water content in the upper mantle, *in* Eiler, J.M., ed., Inside the Subduction Factory: Washington, D.C., American Geophysical Union Geophysical Monograph 138, p. 135–152.

Khan, P.K., and Chakraborty, P.P., 2005, Two-phase opening of Andaman Sea: A new seismotectonic insight: Earth and Planetary Science Letters, v. 229, p. 259–271, doi:10.1016/j.epsl.2004.11.010.

Kneller, E.A., Long, M.D., and van Keken, P.E., 2008, Olivine fabric transitions and shear wave anisotropy in the Ryukyu subduction system: Earth and Planetary Science Letters, v. 268, p. 268–282, doi:10.1016/j.epsl.2008.01.004.

Le Dain, A.Y., Tapponnier, P., and Molnar, P., 1984, Active faulting and tectonics of Burma and surrounding regions: Journal of Geophysical Research, v. 89, p. 453–472, doi:10.1029/JB089iB01p00453.

Lev, E., Long, M.D., and Van der Hilst, R.D., 2006, Seismic anisotropy in eastern Tibet from shear wave splitting reveals changes in lithospheric deformation: Earth and Planetary Science Letters, v. 251, p. 293–304, doi:10.1016/j.epsl.2006.09.018.

Li, C., Van de Hilst, R.D., Meltzer, A.S., and Engdahl, E.R., 2008, Subduction of the Indian lithosphere beneath the Tibetan Plateau and Burma: Earth and Planetary Science Letters, v. 274, p. 157–168, doi:10.1016/j.epsl.2008.07.016.

Liu, K.H., Gao, S., Gao, Y., and Wu, J., 2008, Shear wave splitting and mantle flow associated with the deflected Pacific slab beneath northeast Asia: Journal of Geophysical Research, v. 113, doi:10.1029/2007JB005178.

Mainprice, D., and Silver, P.G., 1993, Interpretation of SKS-waves using samples from the subcontinental lithosphere: Physics of the Earth and Planetary Interiors, v. 78, p. 257–280, doi:10.1016/0031-9201(93)90160-B.

Maury, R.C., Pubellier, M., Rangin, C., Wulput, L., Cotten, J., Socquet, A., Bellon, H., Guillaud, J.-P., and Htun, H.M., 2004, Quaternary calc-alkaline and alkaline volcanism in an hyper-oblique convergence setting, central Myanmar and western Yunnan: Bulletin de la Société Géologique de France, v. 175, p. 461–472, doi:10.2113/175.5.461.

Meade, C., Silver, P.G., and Kaneshima, S., 1995, Laboratory and seismological observations of lower mantle isotropy: Geophysical Research Letters, v. 22, p. 1293–1296, doi:10.1029/95GL01091.

Michel, G.W., Yu, Y.Q., Zhu, S.Y., Reigber, C., Becker, M., Reinhart, E., Simons, W., Ambrosius, B., Vigny, C., Chamot-Rooke, N., Le Pichon, X., Morgan, P., and Matheussen, S., 2001, Crustal motion and block behavior in SE-Adia from GPS measurements: Earth and Planetary Science Letters, v. 187, p. 239–244.

Molnar, P., and Tapponnier, P., 1975, Cenozoic tectonics of Asia: Effects of a continental collision: Science, v. 189, p. 419–426, doi:10.1126/science.189.4201.419.

Molnar, P., and Tapponnier, P., 1977, Relation of the tectonics of eastern China to the India-Eurasia collision: Application of slip-line field theory to large-scale continental tectonics: Geology, v. 5, p. 212–216, doi:10.1130/0091-7613(1977)5<212:ROTTOE>2.0.CO;2.

Najman, Y., Bickle, M., BouDagher-Fadel, M., Carter, A., Garzanti, E., Paul, M., Wijbrans, J., Willett, E., Oliver, G., Parrish, R., Akhter, S.H., Allen, R., Ando, S., Chisty, E., Reisberg, L., and Vezzoli, G., 2008, The Paleogene record of Himalayan erosion: Bengal Basin, Bangladesh: Earth and Planetary Science Letters, v. 273, p. 1–14, doi:10.1016/j.epsl.2008.04.028.

Ni, J.F., Guzman-Speziale, M., Bevis, M., Holt, W.E., Wallace, T.C., and Seager, W.R., 1989, Accretionary tectonics of Burma and the three-dimensional geometry of the Burma subduction zone: Geology, v. 17, p. 68–71, doi:10.1130/0091-7613(1989)017<0068:ATOBAT>2.3.CO;2.

Nicolas, A., and Christensen, N.I., 1987, Formation of anisotropy in upper mantle peridotites—A review, *in* Fuchs, K., and Froidevaux, C., eds., Composition, Structure, and Dynamics of the Lithosphere-Asthenosphere System: Washington, D.C., American Geophysical Union Geodynamics Series, v. 16, p. 111–123.

Nielsen, C., Chamot-Rooke, N., Rangin, C., and the ANDAMAN Cruise Team, 2004, From partial to full strain partitioning along the Indo-Burmese hyperoblique subduction: Marine Geology, v. 209, p. 303–327, doi:10.1016/j.margeo.2004.05.001.

Oreshin, S., Vinnik, L., Makayeva, L., Kosarev, G., Kind, R., and Wentzel, F., 2002, Combined analysis of SKS splitting and regional P traveltimes in Siberia: Geophysical Journal International, v. 151, p. 393–402.

Patzelt, A., Li, H., Wang, J., and Appel, E., 1996, Paleomagnetism of Cretaceous to Tertiary sediments from southern Tibet: Evidence for the extent of the northern margin of India prior to the collision with Eurasia: Tectonophysics, v. 259, p. 259–284, doi:10.1016/0040-1951(95)00181-6.

Ramsay, J.G., and Lisle, R.J., 2000, The Techniques of Modern Structural Geology, Vol. 3: Applications of continuum mechanics in structural geology: London, Academic Press, 360 p.

Rao, N.P., and Kalpna, 2005, Deformation of the subducted Indian lithospheric slab in the Burmese Arc: Geophysical Research Letters, v. 32, p. L05301, doi:10.1029/2004GL022034.

Restivo, A., and Helffrich, G., 1999, Teleseismic shear wave splitting measurements in noisy environments: Geophysical Journal International, v. 137, p. 821–830, doi:10.1046/j.1365-246x.1999.00845.x.

Ribe, N.M., 1989a, A continuum theory for lattice preferred orientation: Geophysical Journal International, v. 97, p. 199–207, doi:10.1111/j.1365-246X.1989.tb00496.x.

Ribe, N.M., 1989b, Seismic anisotropy and mantle flow: Journal of Geophysical Research, v. 94, p. 4213–4223, doi:10.1029/JB094iB04p04213.

Ribe, N.M., and Yu, Y., 1991, A theory for plastic deformation and textural evolution of olivine polycrystals: Geophysical Journal International, v. 94, p. 4213–4223.

Russo, R.M., 2009, Subducted oceanic asthenosphere and upper mantle flow beneath the Juan de Fuca slab: Lithosphere, v. 1, p. 195–205, doi:10.1130/L41.1.

Russo, R.M., and Mocanu, V.I., 2009, Source-side shear wave splitting and upper mantle flow in the Romanian Carpathians and surroundings: Earth and Planetary Science Letters, v. 287, p. 205–216, doi:10.1016/j.epsl.2009.08.028.

Russo, R.M., and Silver, P.G., 1994, Trench-parallel mantle flow beneath the Nazca plate: Results from seismic anisotropy: Science, v. 263, p. 1105–1111, doi:10.1126/science.263.5150.1105.

Russo, R.M., Speed, R.C., Okal, E.A., Shepherd, J.B., and Rowley, K.C., 1993, Seismicity and tectonics of the southeastern Caribbean: Journal of Geophysical Research, v. 98, p. 14,299–14,319, doi:10.1029/93JB00507.

Geosphere, published online on 12 January 2012 as doi:10.1130/GES00534.1




Russo, R.M., Gallego, A., Comte, D., Mocanu, V., Murdie, R.E., and VanDecar, J.C., 2010, Source-side shear wave splitting and upper mantle flow in the Chile Ridge subduction region: Geology, v. 38, p. 707–710, doi:10.1130/G30920.1.

Saltzer, R.L., Gaherty, J.B., and Jordan, T.H., 2000, How are vertical shear wave splitting measurements affected by variations in the orientation of azimuthal anisotropy with depth?: Geophysical Journal International, v. 141, p. 374–390, doi:10.1046/j.1365-246x.2000.00088.x.

Sandvol, E., Ni, J., Ozalaybey, S., and Schue, J., 1992, Shear-wave splitting in the Rio Grande Rift: Geophysical Research Letters, v. 19, p. 2337–2340.

Savage, M.K., 1999, Seismic anisotropy and mantle deformation: What have we learned from shear wave splitting?: Reviews of Geophysics, v. 37, p. 65–106, doi:10.1029/98RG02075.

Savage, M.K., Sheehan, A.F., and Lerner-Lam, A., 1996, Shear wave splitting across the Rocky Mountain Front: Geophysical Research Letters, v. 23, p. 2267–2271.

Schlichting, H., and Gersten, K., 2000, Boundary Layer Theory: Berlin-Heidelberg, Eighth Edition, Springer-Verlag, 801 p.

Schmid, C., van der Lee, S., and Giardini, D., 2004, Delay times and shear wave splitting in the Mediterranean region: Geophysical Journal International, v. 159, p. 275–290.

Shen, Z.-K., Lü, J., Wang, M., and Bürgmann, R., 2005, Contemporary crustal deformation around the southeast borderland of the Tibetan Plateau: Journal of Geophysical Research, v. 110, p. B11409, doi:10.1029/2004JB003421.

Silver, P.G., 1996, Seismic anisotropy beneath the continents: Probing the depths of geology: Annual Review of Earth and Planetary Sciences, v. 24, p. 385–432, doi:10.1146/annurev.earth.24.1.385.

Silver, P.G., and Chan, W.W., 1991, Shear wave splitting and subcontinental mantle deformation: Journal of Geophysical Research, v. 96, p. 16,429–16,454, doi:10.1029/91JB00899.

Simons, W.J.F., Ambrosius, B.A.C., Noomen, R., Angermann, D., Wilson, P., Becker, M., Reinhart, E., Walpersdorf, A., and Vigny, C., 1999, Observing plate motions in southeast Asia: Geodetic results of the GEODYSSEA Project: Geophysical Research Letters, v. 26, p. 2081–2084.

Simons, W.J.F., Socquet, A., Vigny, C., Ambrosius, B.A.C., Haji Abu, S., Promthong, C., Subarya, C., Sarsito, D.A., Matheussen, S., Morgan, P., and Spakman, W., 2007, A decade of GPS in southeast Asia: Resolving Sundaland motion and boundaries: Journal of Geophysical Research, v. 112, p. B06420, doi:10.1029/2005JB003868.

Singh, A., Kumar, M.R., Raju, P.S., and Ramesh, D.S., 2006, Shear wave anisotropy of the northeast Indian lithosphere: Geophysical Research Letters, v. 33, p. L16302, doi:10.1029/2006GL026106.

Singh, A., Kumar, M.R., and Raju, P.S., 2007, Mantle deformation in Sikkim and adjoining Himalaya: Evidences for a complex flow pattern: Physics of the Earth and Planetary Interiors, v. 164, p. 232–241, doi:10.1016/j.pepi.2007.07.003.

Socquet, A., Vigny, C., Chamot-Rooke, N., Simons, W., Rangin, C., and Ambrosius, B., 2006, India and Sunda plates motion along their boundary in Burma determined by GPS: Journal of Geophysical Research, v. 111, p. B05406, doi:10.1029/2005JB003877.

Sol, S., Meltzer, A., Bürgmann, R., van der Hilst, R.D., King, R., Chen, Z., Koons, P.O., Lev, E., Liu, Y.P., Zeitler, P.K., Zhang, X., Zhang, J., and Zurek, B., 2007, Geodynamics of the southeastern Tibetan Plateau from seismic anisotropy and geodesy: Geology, v. 35, p. 563–566, doi:10.1130/G23408A.1.

Stork, A.L., Selby, N.D., Heyburn, R., and Searle, M.P., 2008, Accurate relative earthquake hypocenters reveal structure of the Burma subduction zone: Bulletin of the Seismological Society of America, v. 98, p. 2815–2827.

Tanaka, K., Mu, C., Sato, K., Takemoto, K., Miura, D., Liu, Y., Zaman, H., Yang, Z., Yokoyama, M., Iwamoto, H., Uno, K., and Otofuji, Y., 2008, Tectonic deformation around the eastern Himalayan syntaxis: Constraints from the Cretaceous paleomagnetic data from the Shan-Thai block: Geophysical Journal International, v. 175, p. 713–728, doi:10.1111/j.1365-246X.2008.03885.x.

Tapponnier, P., Peltzer, G., Le Dain, A.Y., Armijo, R., and Cobbold, P., 1982, Propagating extrusion tectonics in Asia: New insights from simple experiments with plasticine: Geology, v. 10, p. 611–616, doi:10.1130/0091-7613(1982)10<611:PETIAN>2.0.CO;2.

Tommasi, A., Tikoff, B., and Vauchez, A., 1999, Upper mantle tectonics: Three-dimensional deformation, olivine crystallographic fabrics and seismic properties: Earth and Planetary Science Letters, v. 168, p. 173–186, doi:10.1016/S0012-821X(99)00046-1.

Van der Lee, S., Regenauer-Lieb, K., and Yuen, D.A., 2008, The role of water in connecting past and future episodes of subduction: Earth and Planetary Science Letters, v. 273, p. 15–27, doi:10.1016/j.epsl.2008.04.041.

Vigny, C., Simons, W.J.F., Abu, S., Bamphenyu, R., Satirapod, C., Choosakul, N., Subarya, C., Socquet, A., Omar, K., Abidin, H.Z., and Ambrosius, B.A.C., 2005, Insight into the 2004 Sumatra-Andaman earthquake from GPS measurements in southeast Asia: Nature, v. 436, p. 201–206, doi:10.1038/nature03937.

Vinnik, L.P., Farra, V., and Romanowicz, B, 1989a, Azimuthal anisotropy in the Earth from observations of SKS at GEOSCOPE and NARS broadband stations: Bulletin of the Seismological Society of America, v. 79, p. 1542–1558.

Vinnik, L.P., Kind, R., Kosarev, G.L., and Makeyeva, L.I., 1989b, Azimuthal anisotropy in the lithosphere from observations of long-period S-waves: Geophysical Journal International, v. 99, p. 549–559, doi:10.1111/j.1365-246X.1989.tb02039.x.

Vinnik, L.P., Makeyeva, L.I., Milev, A., and Usenko, Y., 1992, Global patterns of azimuthal anisotropy and deformation in the continental mantle: Geophysical Journal International, v. 111, p. 433–447, doi:10.1111/j.1365-246X.1992.tb02102.x.

Vinnik, L.P., Krishna, V.G., Kind, R., Bormann, P., and Stammler, K., 1994, Shear wave splitting in the records of the German Regional Seismic Network: Geophysical Research Letters, v. 21, p. 457–460, doi:10.1029/94GL00396.

Walker, K.T., Nyblade, A.A., Klemperer, S.L., Bokelman, G.H.R., and Owens, T.J., 2004, On the relationship between extension and anisotropy: Constraints from shear wave splitting across the East African Plateau: Journal of Geophysical Research, v. 109, doi:10.1029/2003JB002866.

Wang, C.-Y., Flesch, L.M., Silver, P.G., Chang, L.-J., and Chan, W.W., 2008, Evidence for mechanically coupled lithosphere in central Asia and resulting implications: Geology, v. 36, p. 363–366, doi:10.1130/G24450A.1.

Wiejacz, P., 2001, Shear wave splitting across Tornquist-Teisseyre zone in Poland: Journal of the Balkan Geophysical Society, v. 4, p. 91–100.

Wookey, J., and Kendall, J.-M., 2004, Evidence of midmantle anisotropy from shear wave splitting and the influence of shear-coupled *P* waves: Journal of Geophysical Research, v. 109, p. B07309, doi:10.1029/2003JB002871.

Wylegalla, K., Bock, G., Gossler, J., and Hanka, W., 1999, Anisotropy across the Sorgenfrei-Tornquist Zone from shear wave splitting: Tectonophysics, v. 314, p. 335–350, doi:10.1016/S0040-1951(99)00252-8.

Zhang, P.-Z., Shen, Z., Wang, M., Gan, W., Burgmann, R., Molnar, P., Wang, Q., Niu, Z., Sun, J., Wu, J., Hanrong, S., and Xinzhao, Y., 2005, Continuous deformation of the Tibetan Plateau from global positioning system data: Geology, v. 39, p. 809–812.

Zhang, S., Karato, S., Fitzgerald, J., Faul, U.H., and Zhou, Y., 2000, Simple shear deformation of olivine aggregates: Tectonophysics, v. 316, p. 133–152, doi:10.1016/S0040-1951(99)00229-2.

Zhao, L., Jordan, T.H., and Chapman, C.H., 2000, Three-dimensional Fréchet differential kernels for seismic delay times: Geophysical Journal International, v. 141, p. 558–576, doi:10.1046/j.1365-246x.2000.00085.x.


MANUSCRIPT RECEIVED 15 JULY 2009
REVISED MANUSCRIPT RECEIVED 26 SEPTEMBER 2011
MANUSCRIPT ACCEPTED 16 OCTOBER 2011